HOLE FORMATION IN FREELY-STANDING POLYSTYRENE FILMS

A Thesis

Presented to

The Faculty of Graduate Studies

of

The University of Guelph

by

CONNIE B. ROTH

In partial fulfilment of requirements

for the degree of

Master of Science

August, 1999

ABSTRACT

HOLE FORMATION IN FREELY-STANDING POLYSTYRENE FILMS

Connie B. Roth
University of Guelph, 1999

Advisor:
Professor J.R. Dutcher

We have developed a sensitive experiment which allows us to observe the onset of hole formation in thin freely-standing polystyrene (PS) films. In the experiment, a constant small pressure difference is applied and maintained across the freely-standing film held at a fixed elevated temperature. The formation of holes due to the thermal instability of the film is detected as a flow of air through the film. We have studied the onset of hole formation in very thin, freely-standing PS films for which the glass transition temperature T_g is 40°C less than the bulk value of T_g (bulk) = 98°C. For these films, we observed hole formation, and therefore substantial chain mobility, at temperatures that are less than the bulk value of T_g. However, hole formation is only observed at temperatures that are substantially higher than the T_g value of the films.

Acknowledgements

As all things in life go, no one ever accomplishes anything of significance alone. This masters thesis is no exception.

During the past two years it has been a pleasure to be a part of the Guelph BLS Polymer Group. Our supervisor, John Dutcher leads by example, always putting in more effort than is required. John has been patient (during those few stressful weeks before the APS meeting when I was having difficulty making samples), experienced ("now is the time to concentrate on preparing the talk and no longer on collecting data") and supportive ("You'll be well enough on Thursday to give the talk, right?"). I am grateful to John for reading this thesis so carefully; although frustrating at times, I know that it has made me a better writer. Thanks for making the last two years a fulfilling and challenging experience.

Kari Dalnoki-Veress was invaluable during the building of the experiment and collecting of data. He was always willing to answer my many questions and be supportive when things were not working as smoothly as I thought they should. Through Kari, I was able to see how everything was eventually going to come together. He has left big shoes to fill and I hope my feet will one day grow into them.

Chris, Chris and Chris — I would like to thank Christian Gigault for being an excellent walking encyclopedia on electronics, C programming and LaTeX syntax. Chris Schultz-

Nielsen has provided plenty of distractions to ensure that I get those much needed breaks from writing, while Chris Murray's tireless work habits remind me to keep focused.

I am grateful to Professor Bernie Nickel for useful discussions and his help on the calculation of the fitting function (who knew $PV = nRT$ could be so complicated). I acknowledge Professor Jim Stevens for reading this thesis and Professor Ross Hallett for being on the examining committee.

I would also like to thank all the guys in the machine shop: Bill Morton, who taught me how to machine, and all the other guys (Tony, Case, Terry, and Tom) who allowed me to bother them endlessly with questions. Without their help I would not have had an experiment in the first place.

To my mother Anita and brother Tom, I am grateful for support, encouragement and understanding when I was too busy to come home for a visit. Jen DeBoer has been there in spirit for every word I have written and for her email support during the writing of this thesis I am grateful. A special thanks should go to Brian McAneney for teaching me the joy of experiments and introducing me to polymers. And finally I wish to thank Nick Alessi who got me to enjoy the rest of my life as much as I enjoy physics.

To all those that I have encountered .... Thanks.

Contents

List of figures

List of tables

1 Introduction

Thin, freely-standing liquid films are unstable to the formation of holes. The most familiar example of this instability is the bursting of a soap bubble. The instability occurs because thermal fluctuations of the film surfaces can be amplified by the attractive van der Waals or dispersion interaction for which it is energetically favorable to bring the two film surfaces together. At sufficiently long wavelengths, the decrease in free energy due to the dispersion interaction is greater than the energy cost of creating new surface, as determined by the surface tension, resulting in hole formation and growth with time [1].

1.1 Mobility of Polymer Molecules in Bulk

Typically, the mobility of polymer molecules is determined by the material's temperature relative to the glass transition temperature T_g. In very simple terms, T_g is the temperature at which the polymer goes from being in a hard glassy state to a soft rubbery state. In principle, at temperatures above T_g the polymer molecules are free to move whereas below T_g they are frozen in place. Experimentally, T_g is determined by measuring the temperature at which a discontinuity occurs in the thermal expansion or heat capacity of the material. At the molecular level, this discontinuity in the polymer's properties occurs upon heating when enough thermal energy is available to allow segmental rotations about the backbone. Thus, the glass transition temperature is a measure of the movement and

rotations of polymer segments, i.e. *segmental* mobility.

Translation and diffusion of entire polymer molecules, i.e. *chain* mobility, is described by a polymer's viscosity. For many polymers, the temperature dependence of the viscosity is described by the empirical 'Vogel-Fulcher law' [2]

$$\eta(T) = Be^{\frac{T_A}{T-T_V}}. \tag{1.1}$$

Apart from the prefactor B, the Vogel-Fulcher function has two parameters: the 'Vogel temperature' T_V and 'activation temperature' T_A. T_A is interpreted as an activation energy for chain motion, while T_V corresponds, in principle, to the temperature at which the viscosity diverges to infinity and all motions cease. For most practical purposes, motion ceases $\sim$ 50°C above T_V, corresponding to T_g, as the viscosity is very large ($\sim 10^{13}$ poise) and increases rapidly with decreasing temperature. Thus, the singularity at T_V cannot be verified experimentally, but the temperature dependence of the viscosity at temperatures $T > T_g$ can be used to infer the value of T_V: a plot $\ln(\eta)$ versus $1/T$ exhibits a characteristic curvature which distinguishes it from an Arrhenius behaviour [2].

Measurements of the creep compliance $J(t)$, performed by applying a constant stress and measuring the time dependent strain of the material, are useful in the understanding of the different types of mobility of the molecules. The general shape of a so-called 'creep compliance curve' is illustrated in Figure 1.2. There are four main regions of the creep compliance curve that are common to all polymers: the glassy region, the glass-rubber transition, the rubber-elastic plateau, and the terminal flow region. For example, such curves have been measured experimentally for polystyrene [2]. By measuring $J(t)$ at different temperatures between -268°C and 296.5°C, and using time-temperature super-

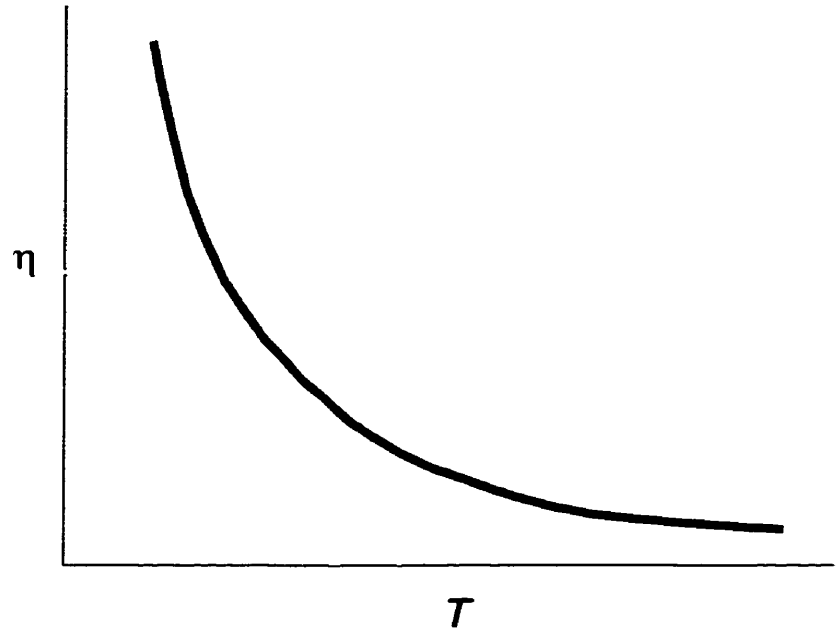

Figure 1.1: Schematic diagram of viscosity η versus temperature T following the Vogel-Fulcher function.

position, the entire creep compliance curve can be measured. By varying the temperature, different parts of the $J(t)$ creep curve show up in the time-window of the experiment.

The transition from the glassy region to terminal flow occurs continuously starting with the glass-rubber transition. The creep compliance $J(t)$ then undergoes a plateau before reaching the terminal flow region. This rubber-elastic plateau reveals a great deal about the nature of polymer mobility. For instance, the height of the plateau is comparable to the compliance in rubbers suggesting that entanglements in polymer melts act as temporary cross-links. The width of the plateau increases with increasing molecular weight M_w implying that the time needed for chain disentangling increases with M_w. Accordingly, the plateau vanishes upon decreasing M_w, indicating the absence of an entanglement network for low M_w values, and a merging of the glass-rubber transition and the terminal flow region. The terminal flow region is marked by a linear increase of J with time which

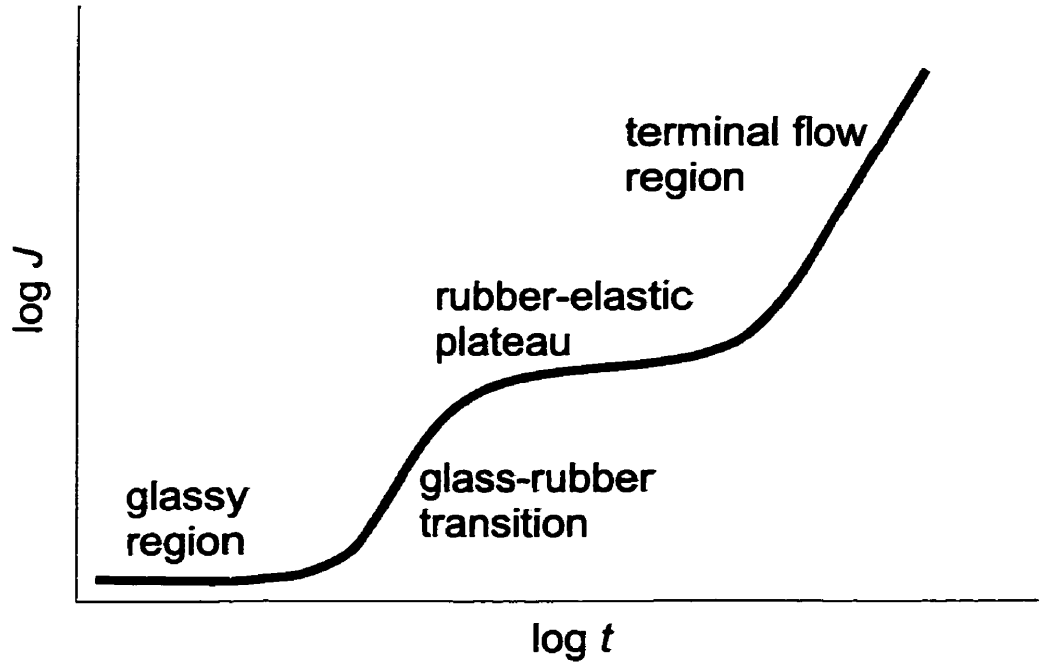

Figure 1.2: General shape of the complete creep compliance $J(t)$ for polymers constructed from data collected on polystyrene measured at different temperatures [2].

is characteristic of viscous flow,

$$\frac{dJ}{dt} \sim \frac{1}{\eta_o}. \tag{1.2}$$

For high M_w values, i.e. for entangled melts, the viscosity η is found to scale very strongly with molecular weight,

$$\eta \sim M_w^{3.4}, \tag{1.3}$$

whereas for low M_w values, $\eta \sim M_w$. Thus, the creep curve of high M_w polymers of Figure 1.2 describes a two step relaxation process. The first occurs at the glass-rubber transition, with relaxations occuring on a segmental length scale. The second relaxation process is highly M_w dependent and takes place on a much longer time scale corresponding to the disentangling of entire chains (*chain* mobility).

The viscosity of polymers is further complicated in the presence of high shear stress

which tends to decrease the number density of entanglements between polymer chains [3]. This leads to a decrease in the viscosity with increasing shear strain rate, $\eta(\dot{\gamma})$, an effect commonly referred to as 'shear thinning'. Figure 1.3 shows the characteristic behaviour of viscosity η for increasing shear strain rate $\dot{\gamma}$. At small values of $\dot{\gamma}$, the viscosity is essentially constant and equal to the zero shear rate value η_o. The region in which $\eta \sim \eta_o$ is referred to as the *linear* viscoelastic regime in which the polymer chain diffusion is generally well understood. However, as the shear strain rate $\dot{\gamma}$ is increased, the viscosity decreases as

$$\eta \sim |\dot{\gamma}|^{-d}, \tag{1.4}$$

where the power d is typically between 0.8 and 0.85 for polymer melts. This corresponds to the *nonlinear* viscoelastic regime. Graessley [3] has found that data collected for different polymers, at different temperatures T and for different molecular weights M_w, can be collapsed onto a single master curve by replacing $\eta(\dot{\gamma})$ with a reduced viscosity function $f(\beta)$ given by

$$f(\beta) = \frac{\eta}{\eta_o} \tag{1.5}$$

in which β is a reduced shear rate defined as

$$\beta = \frac{\eta_o M_w \dot{\gamma}}{\rho R T} \tag{1.6}$$

where R is the gas constant and ρ is the density. It is found that nonlinear viscoelastic effects occur for values of $\beta > 10$.

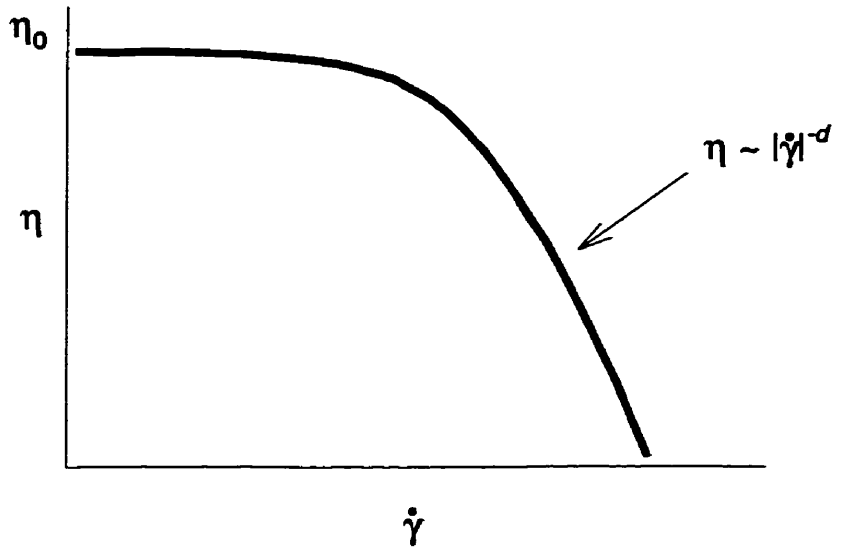

Figure 1.3: Schematic diagram of viscosity η versus shear strain rate $\dot{\gamma}$. Both axes are plotted on a log scale. For large strain rates, the viscosity follows the power law indicated.

1.2 Mobility of Polymer Molecules in Thin Films

1.2.1 Reductions in the Glass Transition Temperature: Segmental Mobility

As mentioned above, the glass transition is associated with segmental mobility. Using Brillouin Light Scattering, our group has measured the glass transition temperature of freely-standing polystyrene (PS) films [4, 5]. By reducing the thickness of the freely-standing films, the polymer molecules are effectively confined in one dimension (the film normal direction). Very large reductions in the glass transition temperature were observed as the film thickness was decreased. Figure 1.4 [5] shows a plot of the glass transition temperature T_g as a function of film thickness h for two different molecular weights: $M_w = 767\times10^3$ (circles) and $M_w = 2240\times10^3$ (triangles). It is observed that confinement of the polymer molecules leads to enhanced segmental mobility.

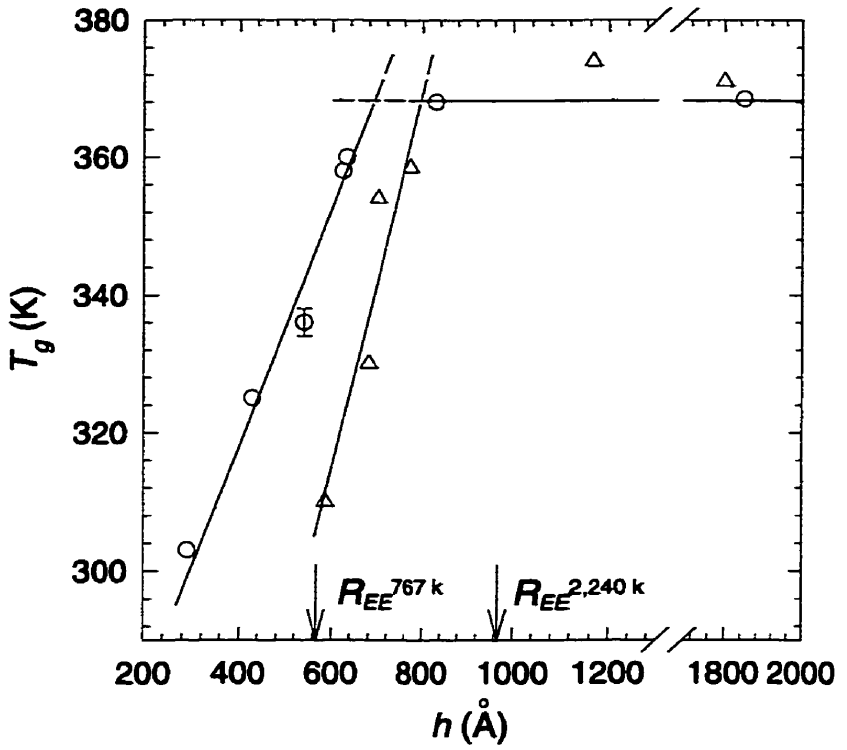

Figure 1.4: Plot showing large reductions in the glass transition temperature T_g as a function of film thickness h for two different molecular weights: $M_w = 767 \times 10^3$ (circles) and $M_w = 2240 \times 10^3$ (triangles). [5]

1.2.2 Hole Formation and Growth: Chain Mobility

Freely-standing polymer films are unstable to the formation of holes at elevated temperatures. There are two ways in which holes can form in freely-standing polymer films, either spontaneously by thermal fluctuations of the film interfaces or by nucleation from a defect or dust spot in the film.

Hole formation and growth in polymer films has been studied previously both by our group [6] and another group from France [7, 8]. It has been shown that the hole radius grows exponentially with time and there is uniform thickening of the film during hole growth for both spontaneous and nucleated holes. The work done by our group [6] used optical microscopy to study hole growth in freely-standing PS films of $M_w = 767 \times 10^3$

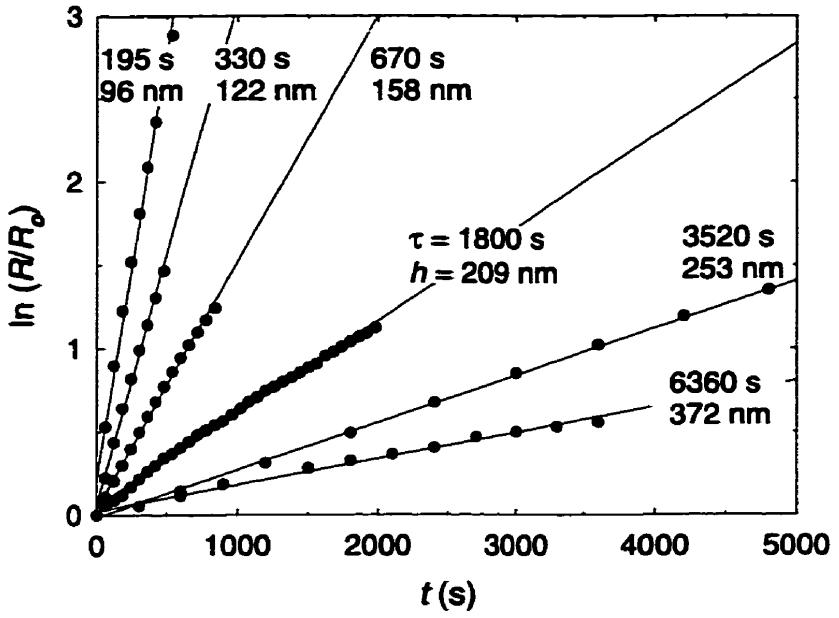

Figure 1.5: Plot of the natural logarithm of the hole radius $\mathcal{R}$, normalized to the value of the radius $\mathcal{R}_o$ first measured for each hole, as a function of time for six representative PS films ranging in film thickness from $h = 96$ nm to 372 nm. The τ and h values are listed for each data set. [6]

that were held at a fixed temperature $T = 115°$C which is only $\sim 17°$C greater than the bulk value of the glass transition temperature $T_g = (98 \pm 2)°$C. Figure 1.5 [6] shows a plot of the natural logarithm of the hole radius $\mathcal{R}$, normalized to the value of the radius $\mathcal{R}_o$ first measured for each hole, as a function of time. The data on this semi-log plot follow straight lines indicating exponential growth of the hole radius,

$$\mathcal{R}(t) = \mathcal{R}_o \, e^{t/\tau}, \tag{1.7}$$

where τ is the characteristic growth time of the holes. The hole growth process in freely-standing polymer films occurs very slowly because of the large values of viscosity. Typically, the velocity with which the hole radius increases is on the order of tens of nm/s, which is about nine orders of magnitude less than the growth velocity for the rupture of soap films [9].

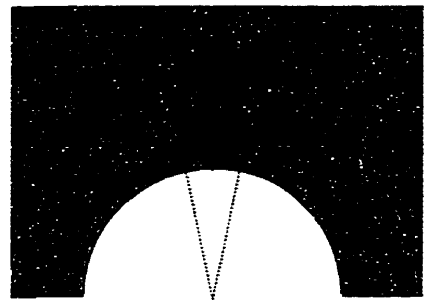

Figure 1.6: Schematic of a film element near the edge of a hole undergoing shear stress. See text for explanation.

Holes in a freely-standing PS film of thickness h grow with time because of the presence of a shear stress

$$\sigma = \frac{2\epsilon}{h} \tag{1.8}$$

due to the surface tension ϵ at the edge of the hole (radial distance $r = \mathcal{R}$). Because σ increases as h decreases, both σ and the resulting shear strain rate $\dot{\gamma}$ can be large for very thin films. To understand the nature of the shear strain associated with the hole growth process, consider an infinitesimal square element of the film at $r = \mathcal{R}$ with one of its diagonals along the radial direction, subtending the angular width $d\theta$ (see Figure 1.6). At a short time later, the same film element has moved outward to $r = \mathcal{R} + d\mathcal{R}$, and the element has been deformed into a parallelogram with its long diagonal perpendicular to the radial direction. This deformation is equivalent to a shear strain.

By measuring the rate of hole growth in the freely-standing PS films, i.e. determining the characteristic growth time τ of the holes, it is possible to get a measure of the viscosity at the edge of the hole. The shear strain γ at the edge of the hole is given by

$$\gamma = 2\,\frac{d\mathcal{R}}{\mathcal{R}} \quad . \tag{1.9}$$

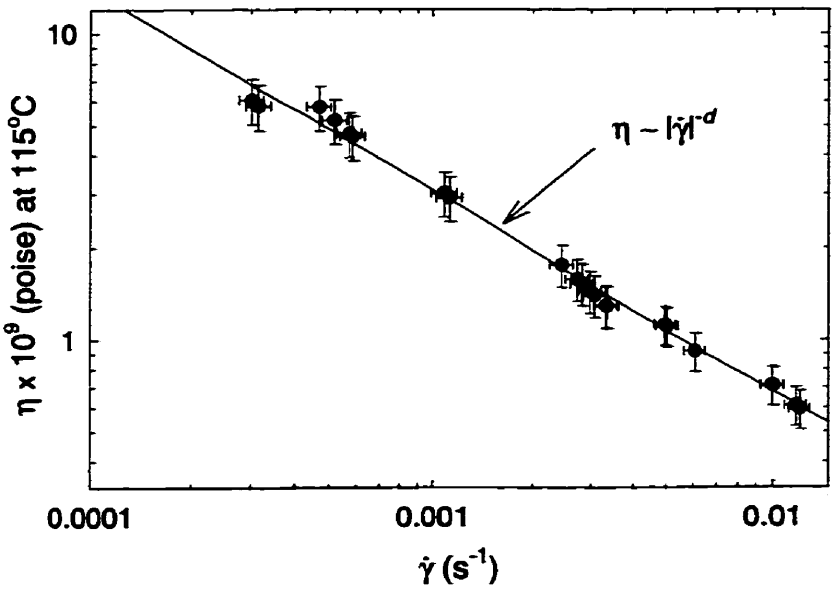

Figure 1.7: Viscosity η at $T = 115°C$ versus the shear strain rate $\dot{\gamma}$. The straight line corresponds to the best fit to $\eta \sim |\dot{\gamma}|^{-d}$, with $d = 0.65 \pm 0.03$. [6]

Using equation (1.7) we can write the shear strain rate $\dot{\gamma}$ as

$$\dot{\gamma} = \frac{2}{\tau} \quad . \tag{1.10}$$

From the definition of viscosity, stress (eqn 1.8) and the strain rate (eqn 1.10), we arrive at

$$\eta = \frac{\sigma}{\dot{\gamma}} = \frac{\tau\epsilon}{h} \quad . \tag{1.11}$$

In the hole growth study done by our group [6], the characteristic growth time τ was measured in 25 different PS films ranging in thickness from $h = 96$ nm to $h = 372$ nm. A plot of viscosity η as a function of shear strain rate $\dot{\gamma}$, shown in Figure 1.7, was obtained as outlined above. The data, shown on a log-log plot, was fit to a straight line corresponding to the best fit to the power law in equation (1.4). By comparing Figure 1.7 to the schematic of a typical plot of viscosity as a function of strain rate in Figure 1.3, we can infer that these hole growth measurements correspond to the nonlinear viscoelastic

regime. This conclusion was verified by calculating the β value, equation (1.6), which was found to range from ~ 40 to ~ 1500. There is a difference between the fitted value of d for the freely-standing PS film and that obtained for bulk PS. This difference occurs because of the radial dependence in the viscosity in the vicinity of the hole edge caused by the radial dependence of the shear strain rate that is present in the nonlinear viscoelastic regime. The measured viscosity in the hole growth experiments is an average viscosity in the vicinity of the edge of the hole.

2 Experimental Techniques

2.1 Description of Differential Pressure Experiment

We have developed a simple Differential Pressure Experiment (DPE) which allows us to maintain a very small pressure difference ΔP across a freely-standing polystyrene (PS) film (for a schematic diagram of the experiment, see Figure 2.1). To maintain the small pressure difference we have built a pressure cell which is divided into two compartments of nearly equal volume (see section A.6). There is a single hole separating the two compartments of the cell. By placing a freely-standing film across this hole, the film separates the two compartments of the pressure cell. A very sensitive pressure sensor which has a resolution of 0.001 torr (section A.5) is used to continuously monitor ΔP. The pressure difference across the PS film is actively stabilized using a computer-controlled pressure feedback system consisting of the differential pressure sensor and a piston (section A.7) connected to the lower compartment of the pressure cell. The position of the piston is controlled by a stepper motor for which each microstep is equal to 0.1 μm (section A.3). The temperature of the pressure cell, and therefore of the PS film, is controlled using a Eurotherm temperature controller to within ± 0.5°C. To isolate the system from slight variations in room temperature as well as the heated pressure cell, we have enclosed the Differential Pressure Experiment, with the exception of the pressure cell, in a thermally-

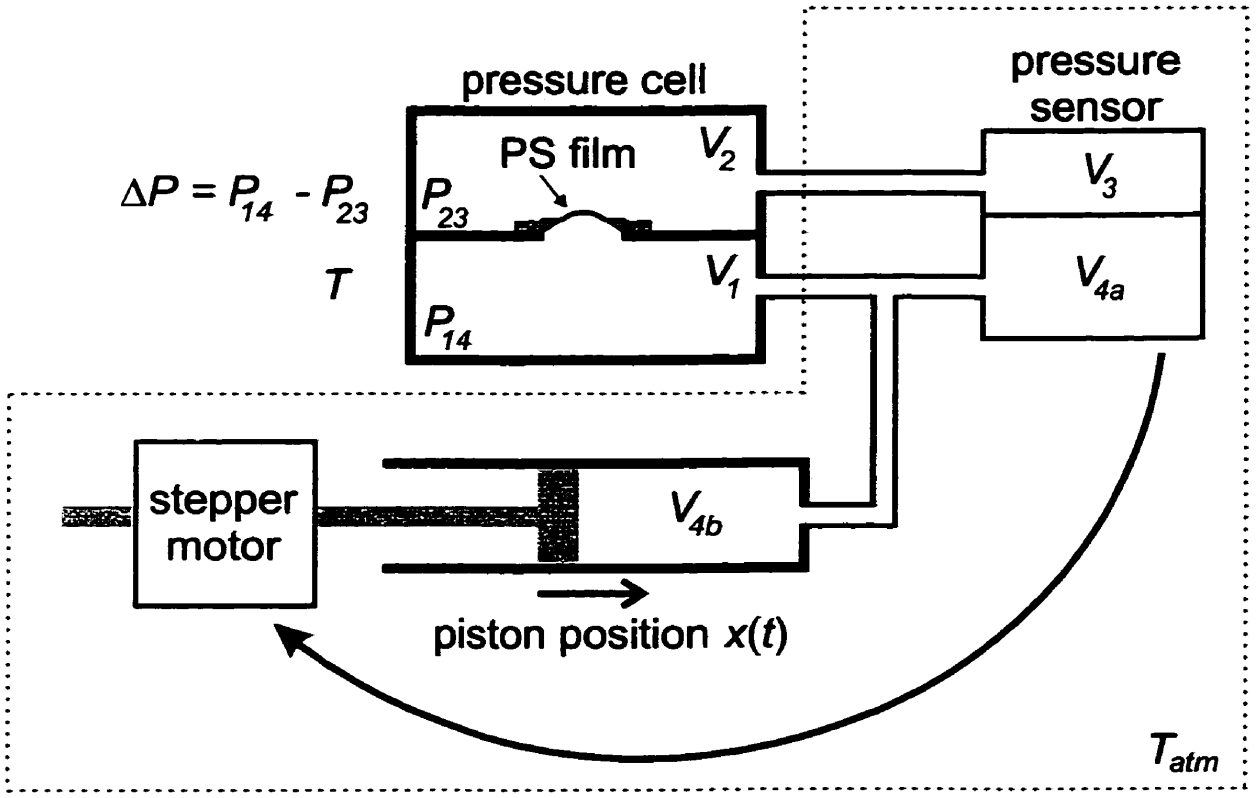

Figure 2.1: Schematic diagram of the Differential Pressure Experiment showing relevant variables.

insulated box.

Typically for the DPE experiments described in this thesis we fix the temperature T of the pressure cell, which is equal to the temperature of the sample, we maintain a very small pressure difference ($\Delta P < 10$ Pa), and we simply track the position of the piston $x(t)$ as a function of time. When holes start to form in the freely-standing film, air flows across the film and the piston has to continuously drift forward to maintain the pressure difference across the film.

In previous hole formation studies [6] performed on thicker polystyrene films (film thickness $h > 96$ nm) with bulk values of T_g, hole formation and growth was observed at a temperature ~ 18°C above the bulk value of T_g. This measurement was performed

using optical microscopy which has a maximum spatial resolution of ~ 0.2 μm over a small portion of the entire film. Other techniques, such as Atomic Force Microscopy (AFM), have better spatial resolution (~ 1 nm), but only over a smaller portion of the entire film. The Differential Pressure Experiment is unique in that it is able to detect the formation of small holes over the entire film surface. The DPE is sensitive to total hole areas of ~ 30 μm^2 over the entire surface of the film (4 mm in diameter). To give the reader a feel for the typical hole size to which this corresponds, we can estimate a typical initial hole diameter of ~ 20 nm by dividing the total hole area by the hole density observed in Figure 3.4 (~ 13000 holes/mm^2).

The concept of the DPE is similar to that used previously to study the room-temperature mechanical properties of thin plates and membranes [10, 11]. In these measurements, the film deflection at the center of the film was measured as a function of a large applied pressure difference (typically 10 kPa) to infer the Young's modulus of the film.

2.2 Analysis of Differential Pressure Experiment

2.2.1 Flow of Gas Through Holes

Effusion is the process by which gas passes through a very small hole. In this process it is assumed that the gas molecules do not collide with each other as they pass through the hole, such that every molecule that impinges on the hole will pass through it.

Effusion is valid in the limit that the hole diameter is less than the mean free path ℓ of the gas molecules, which for nitrogen at atmospheric pressure and 95°C is $\ell = 0.3$ μm. Since we are concerned with measuring the onset of hole formation in freely-standing polymer films with hole diameters much less than 1 μm, we will be well within the effusion

limit for the initial stages of hole growth.

The effusion approximation will break down if the hole diameters are comparable to or greater than ℓ. Also, as holes grow large, uniform thickening of the film occurs which changes the characteristic growth time $\tau(h)$ (see section 1.2.2). This effect will be negligible until the total hole area comprises more than 5% of the total film surface (4 mm in diameter).

In the effusion limit, the flux I through a hole is defined as the number of molecules crossing the hole per second per unit area of the hole. We can write this as the integral over momentum of the product of the velocity v_x and the momentum distribution $f(\mathbf{p})$ of the velocities [12]

$$I = \int_{v_x>0} d^3p\, v_x\, f(\mathbf{p}). \tag{2.1}$$

Note we have taken the x-axis to be perpendicular to the hole. Assuming a Maxwell-Boltzmann distribution for the momentum of molecules of mass m and density ρ:

$$f(\mathbf{p}) = \frac{\rho}{(2\pi mkT)^{3/2}}\, e^{-\mathbf{p}^2/2mkT} \tag{2.2}$$

$$= \frac{\rho}{(2\pi mkT)^{3/2}}\, e^{-m\mathbf{v}^2/2kT}, \tag{2.3}$$

the flux I becomes

$$I = \frac{\rho m^3}{(2\pi mkT)^{3/2}} \int_0^\infty dv_x\, v_x\, e^{-m\bar{v_x}^2/2kT} \int_{-\infty}^\infty dv_y\, e^{-m\bar{v_y}^2/2kT} \int_{-\infty}^\infty dv_z\, e^{-m\bar{v_z}^2/2kT}, \tag{2.4}$$

which simplifies to

$$I = \rho\sqrt{\frac{kT}{2\pi m}}. \tag{2.5}$$

Using the ideal gas law, $PV = NkT$, we can replace the density $\rho = N/V$ to get

$$I = \frac{P}{\sqrt{2\pi mkT}}. \tag{2.6}$$

With reference to the schematic of the experiment (Fig. 2.1), there will be a flux of molecules $I_{\uparrow}$ from the 'bottom' compartment of the cell of volume V_1 to the 'top' compartment of the cell of volume V_2 that depends on the pressure P_{14} in the 'bottom' compartment of the cell:

$$I_{\uparrow} = \frac{P_{14}}{\sqrt{2\pi mkT}}, \tag{2.7}$$

where T is the cell temperature. There will also be a flux of molecules $I_{\downarrow}$ from the 'top' compartment of the cell to the 'bottom' compartment of the cell that depends on the pressure P_{23} in the 'top' compartment:

$$I_{\downarrow} = \frac{P_{23}}{\sqrt{2\pi mkT}}. \tag{2.8}$$

Since $P_{14} = P_{23} + \Delta P$, where ΔP is the pressure difference between the two compartments of the cell, there will be a net flux ΔI between the two compartments given by

$$\Delta I = \frac{\Delta P}{\sqrt{2\pi mkT}}. \tag{2.9}$$

The number of molecules δN passing through the polymer film as a function of time will be given by the integral over time of the net flow ΔI times the total hole area $A_h(t)$:

$$\delta N(t) = \int_0^t \Delta I \; A_h(t')\, dt'. \tag{2.10}$$

As discussed in section 1.2.2, from previous work [6], we know that the radius r of each hole grows exponentially with time: $r(t) = r_o e^{t/\tau}$, where τ is the characteristic growth time and r_o is the initial hole radius. All holes grow with the same characteristic growth time τ, which depends only on the viscosity η, thickness h and surface tension ϵ (see eqn. 1.11). Thus, if n is the total number of holes, we have

$$A_h(t) = n\pi[r(t)]^2 = \pi e^{2t/\tau}(nr_o^2). \tag{2.11}$$

Of course, not all holes form at the same time or with the same initial radius. Because of this, equation (2.11) should read

$$A_h(t) = \sum_{i=1}^{n} \pi \, r_{oi}^2 \, e^{2(t-t_i)/\tau} \tag{2.12}$$

where the ith hole begins with a radius r_{oi} at time t_i. However, the time dependence can be factored out of the sum in eqn. (2.12) such that it is of the same form as eqn. (2.11):

$$A_h(t) = \pi e^{2t/\tau} \left[\sum_{i=1}^{n} r_{oi}^2 e^{-2t_i/\tau} \right] . \tag{2.13}$$

Thus, equation (2.10) becomes

$$\delta N(t) = \int_0^t \Delta I \, A_h(t) \, dt \tag{2.14}$$

$$= \int_0^t \left(\frac{\Delta P}{\sqrt{2\pi m k T}} \right) \pi \, e^{2t/\tau} \left[\sum_{i=1}^{n} r_{oi}^2 e^{-2t_i/\tau} \right] dt \ . \tag{2.15}$$

For fixed ΔP, we can write

$$\delta N(t) = \frac{\Delta P}{\sqrt{2\pi m k T}} \pi \left[\sum_{i=1}^{n} r_{oi}^2 e^{-2t_i/\tau} \right] \underbrace{\int_0^t e^{2t/\tau} \, dt}_{\frac{\tau}{2}\left(e^{2t/\tau}-1\right)} \ . \tag{2.16}$$

This gives us an expression for the number of molecules $\delta N(t)$ passing through the polymer film as holes grow as a function of time, which depends linearly on the pressure difference ΔP and characteristic growth time τ.

2.2.2 Time Dependence of Piston Position

At the beginning of the Differential Pressure Experiment, before holes form in the polymer film, the initial number of molecules $N_{23}(0)$ in the volumes V_2 and V_3, in contact with the upper surface of the polymer film, is given by the equation of state (for variable names

see Figure 2.1),

$$N_{23}(0) = P_{23}(0)\left(\frac{V_2}{kT} + \frac{V_3}{kT_{atm}}\right), \tag{2.17}$$

and similarly for volumes V_1 and V_4, in contact with the lower surface of the polymer film,

$$N_{14}(0) = P_{14}(0)\left(\frac{V_1}{kT} + \frac{V_4}{kT_{atm}}\right). \tag{2.18}$$

Maintaining a constant pressure difference ΔP between the two compartments of the cell creates a net flux of molecules from the 'bottom' compartment to the 'top' compartment. Thus, the pressure in volumes V_2 and V_3 will increase due to the flow of air through the holes in the polymer film. We write the time dependence of the pressure $P_{23}(t)$ in volumes V_2 and V_3 as the initial pressure plus a time-dependent increase in pressure $\delta P(t)$:

$$P_{23}(t) = P_{23}(0) + \delta P(t). \tag{2.19}$$

The corresponding increase in the number of molecules in volumes V_2 and V_3 is given by

$$N_{23}(t) = N_{23}(0) + \delta N(t), \tag{2.20}$$

where $\delta N(t)$ is given by equation (2.16). Since

$$N_{23}(t) = P_{23}(t)\left(\frac{V_2}{kT} + \frac{V_3}{kT_{atm}}\right), \tag{2.21}$$

where V_2 and V_3 are independent of time, we can express $\delta P(t)$ in terms of $\delta N(t)$:

$$\delta P(t) = \frac{\delta N(t)}{\frac{V_2}{kT} + \frac{V_3}{kT_{atm}}} \tag{2.22}$$

where $\delta N(t)$ is given by equation (2.16).

We now relate $\delta P(t)$ to $x(t)$, the change of the piston position as a function of time. In the volumes V_1 and V_4, the decrease in the number of molecules $N_{14}(t)$ is given by

$$N_{14}(t) = N_{14}(0) - \delta N(t). \tag{2.23}$$

The equation of state for volumes V_1 and V_4 gives us another expression for $N_{14}(t)$:

$$N_{14}(t) = P_{14}(t)\left(\frac{V_1}{kT} + \frac{V_4(t)}{kT_{atm}}\right). \tag{2.24}$$

Note the time dependence of V_4, because the piston moves to maintain a constant pressure difference ΔP. The time dependence of the volume $V_4(t)$ (volumes V_{4a} and V_{4b} combined) can be written in terms of the piston position $x(t)$ and the piston cross section A_p,

$$V_4(t) = V_4(0) - A_p\, x(t). \tag{2.25}$$

As in equation (2.19), we can write the time dependence of the pressure in the volumes V_1 and V_4 as

$$P_{14}(t) = P_{14}(0) + \delta P(t). \tag{2.26}$$

Combining equations (2.18), (2.23), (2.24), (2.25) and (2.26), we obtain

$$P_{14}(0)\left(\frac{V_1}{kT} + \frac{V_4(0)}{kT_{atm}}\right) - \delta N(t) = [P_{14}(0) + \delta P(t)]\left(\frac{V_1}{kT} + \frac{V_4(0) - A_p x(t)}{kT_{atm}}\right), \tag{2.27}$$

which simplifies to

$$-\delta N(t) = -P_{14}(0)\frac{A_p x(t)}{kT_{atm}} - \delta P(t)\frac{A_p x(t)}{kT_{atm}} + \delta P(t)\left(\frac{V_1}{kT} + \frac{V_4(0)}{kT_{atm}}\right). \tag{2.28}$$

Solving for $x(t)$, we obtain

$$x(t) = \frac{\delta N(t) + \delta P(t)\left(\frac{V_1}{kT} + \frac{V_4(0)}{kT_{atm}}\right)}{\frac{A_p}{kT_{atm}}[P_{14}(0) + \delta P(t)]}, \tag{2.29}$$

which is the position of the piston as a function of time in terms of the change in the number of molecules $\delta N(t)$ from equation (2.16) and the change in pressure $\delta P(t)$ from equation (2.22). Rearranging equation (2.29), we obtain a more useful relationship:

$$x(t) = \left[\frac{\delta P(t)}{P_{14}(0) + \delta P(t)}\right]\left\{\left(\frac{V_1 + V_2}{A_p}\right)\frac{T_{atm}}{T} + \left(\frac{V_3 + V_4(0)}{A_p}\right)\right\}. \tag{2.30}$$

Thus to summarize, we have derived three coupled equations (2.16, 2.22, 2.30)

$$\delta N(t) = \frac{\Delta P}{\sqrt{2\pi mkT}}\pi\left[\sum_{i=1}^{n} r_{oi}^2 e^{-2t_i/\tau}\right]\frac{\tau}{2}\left(e^{2t/\tau}-1\right)$$

$$\delta P(t) = \frac{\delta N(t)}{\left(\frac{V_2}{kT}+\frac{V_3}{kT_{atm}}\right)}$$

$$x(t) = \left[\frac{\delta P(t)}{P_{14}(0)+\delta P(t)}\right]\left\{\left(\frac{V_1+V_2}{A_p}\right)\frac{T_{atm}}{T}+\left(\frac{V_3+V_4(0)}{A_p}\right)\right\}$$

that lead us to a fitting function for the time dependence of the piston position of the form:

$$x(t) = A_1 \times \frac{A_2(e^{2t/\tau}-1)}{P_{14}(0)+A_2(e^{2t/\tau}-1)}, \tag{2.31}$$

where A_1 and A_2 are constants, and τ is the characteristic growth time.

Equation (2.31) has to be slightly modified to include a background signal before it can be used as a fitting function for the data. Experimentally, we have measured the long-term stability of the Differential Pressure Experiment by placing a solid brass piece in place of the polymer film, such that no hole formation occured. We find that there is a small negative drift in the piston position which is approximately proportional to time. We believe this small drift to be caused by an increase in T_{atm} by a few degrees over the course of the experiment. The experimental setup has all components within the dashed lines of Figure 2.1 enclosed in a large box isolating the system from fluctuations in room temperature over the course of the experiment (at times lasting up to 48 hours). The presence of the stepper motor within this box slowly heats up volumes V_3 and V_4 by a few degrees over time. The volume difference between volumes V_3 and V_4 causes the pressure P_{14} to increase more than P_{23} leading to the observed drift in the piston position. We have simulated the observed linear drift by including a small linear increase

of T_{atm} (1°C every 3 hours) in our calculation. The time dependence of $T_{atm}(t)$ should be incorporated directly in the calculation, e.g. equations (2.21) and (2.24), but the addition of a phenomenological small drift term is sufficient to describe the data. Thus, our data is fit to the functional form

$$x(t) = A_1 \times \frac{A_2(e^{2t/\tau} - 1)}{P_{14}(0) + A_2(e^{2t/\tau} - 1)} - C_o t \tag{2.32}$$

where C_o is empirically determined to be ~ 1 μm/s. Equation 2.32 contains four fitting parameters: A_1, A_2, C_o and τ. The pressure $P_{14}(0)$ is taken to be atmospheric pressure.[1]

2.3 Sample Preparation

High molecular weight, monodisperse polystyrene (PS) with molecular weight $M_w = 2240 \times 10^3$ and polydispersity index $M_w/M_n = 1.08$ was used to make freely-standing films. The PS was dissolved in toluene (a good solvent) and then spincoated onto clean freshly-cleaved mica substrates to produce supported films of the desired thickness. To achieve a nominal thickness of 65 nm, a solution of 1.126% PS by mass in toluene was spincoated at 4000 RPM producing films of thickness $h \approx 65$ nm with a sample-to-sample variation of ± 4 nm. The thickness of all films used in the Differential Pressure Experiment were measured using ellipsometry to an accuracy of ± 1 nm. We have measured 18 different freely-standing PS films using the Differential Pressure Experiment with thicknesses between 61 nm and 69 nm.

To prepare freely-standing films, the supported films were annealed at a temperature of 115°C which is well above the bulk glass transition temperature $T_g = 98$°C for PS. The films were annealed under vacuum for 12 hours to allow the polymer chains to relax and

[1] Technically $P_{14}(0) = P_{atm} + \Delta P$, but the difference is negligible.

to drive off any residual solvent. Finally the supported polymer films were cooled to room temperature at a well-defined, slow rate of 1 K/min to ensure a well-defined consistent thermal history for all films. The polymer films were then carefully floated off onto a distilled water surface and captured using a sample holder with a 4 mm diameter hole to produce the freely-standing PS films. Pieces of the spincoated film are also floated onto clean silicon wafers to allow for a determination of the initial film thickness using ellipsometry.

In the sample preparation for this experiment we have used mica substrates, instead of glass slides, because of their superior flatness and the ease with which PS films could be floated onto the water surface. As a result, the freely-standing PS contained very few defects. Defects act as nucleation sites for hole growth and any pre-existing hole or tear in the film prevents the study of the film in the Differential Pressure Experiment. All freely-standing PS films were measured using optical microscopy prior to their study in the Differential Pressure Experiment to ensure that there were not any pre-existing holes or tears.

After a freely-standing film was measured in the Differential Pressure Experiment, it was transferred onto a silicon wafer where the final film thickness was measured using ellipsometry.

3

Results and Discussion

3.1 Experimental Results

Using the Differential Pressure Experiment, we have measured 18 different freely-standing polystyrene films. All of the films were composed of the same polymer (polystyrene with molecular weight $M_w = 2240 \times 10^3$), and all of the same nominal thickness of $h = 65$ nm ± 4 nm (see section 2.3). From previous glass transition temperature measurements of freely-standing PS films of the same M_w value ([5], see section 1.2.1), we know that freely-standing PS films with $h \sim 65$ nm have $T_g \sim 55$°C, which is much less than the bulk value of $T_g = 98$°C.

3.1.1 Differential Pressure Experiment (DPE)

For each run of the DPE, we fix the temperature T of the pressure cell and maintain a small pressure difference (typically $\Delta P = 0.05$ torr $= 7$ Pa) across the polymer film. Holding the temperature and pressure fixed, we simply track the position of the piston $x(t)$ as time progresses. The presence of holes is detected as a continuous drift of the piston which moves to maintain a constant pressure difference across the film, in the presence of the flow of air through the holes in the film.

Initially the film is heated from room temperature up to the measurement tempera-

ture T with both sides of the film exposed to atmospheric pressure ($\Delta P = 0$). Small wrinkles appear due to the differential thermal expansion between the PS film and the stainless steel sample holder. At the fixed measurement temperature, the small pressure difference ($\sim 10^{-4}$ atm) is applied which causes the freely-standing film to bow slightly while maintaining the presence of small wrinkles. We observe by eye that, with the film held at the measurement temperature, the wrinkles in the film disappeared with time, demonstrating substantial polymer chain mobility. For all the films, we observed that the wrinkles disappear before hole formation is measured. As an example, with a sample temperature of 90°C, the wrinkles disappeared after $\sim$ 15 min whereas hole formation occured with a characteristic growth time of $\sim$ 10 h.

Figure 3.1 shows a graph of the time dependence of the piston position $x(t)$. This particular data set was obtained for a film with $h = 63$ nm that was held at a fixed temperature of $T = 93$°C and is representative of all of the data sets. The data clearly indicates the expected trends, showing a small linear drift of the piston position at short times which becomes completely overwhelmed by the large piston movement caused by the formation and exponential growth of holes at longer times (see section 2.2). If we fit all of the data in Fig. 3.1 to eqn. 2.32, there are systematic discrepancies between the data and the calculated curve for intermediate times. Instead, to obtain the calculated curve shown in Fig. 3.1, we fit only the data corresponding to the initial stages of hole formation and growth for which the effusion approximation is known to be valid. It is important to obtain a reliable criterion for selecting the range of data used in the fitting procedure for different data sets. For each data set, we have chosen to limit the range of data in terms of the slope of the $x(t)$ values which is a measure of the instantaneous flow

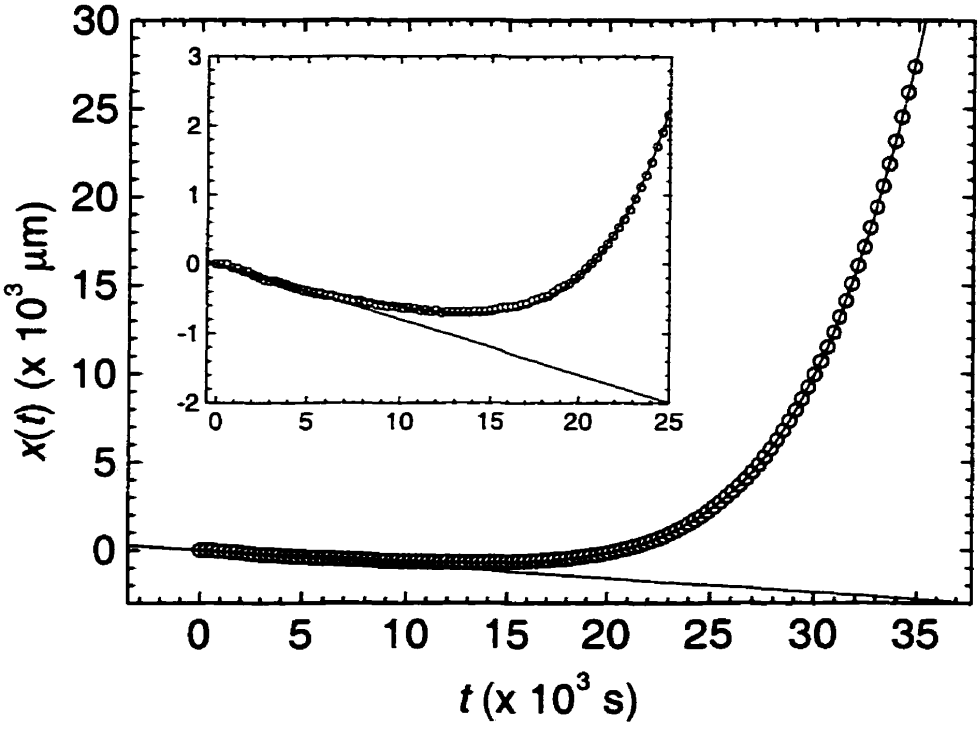

Figure 3.1: Piston position $x(t)$ as a function of time for a 63 nm thick freely-standing polystyrene film held at $T = 93°C$. The open circles correspond to data, and the solid line was calculated using the best fit to eqn. (2.32) using the following parameter values: $\tau = 8560 \pm 10$ s, $A_1 = 0.102 \times 10^6$ μm, $A_2 = 12.3$ Pa and $C_o = 0.0736$ μm/s. The inset shows a magnification of the data and fitted curve for the initial stages of hole growth.

of gas across the film and the total hole area at that time. We have chosen a cutoff value for the slope of 5 μm/s which corresponds to a total hole area of ~ 0.1 mm^2 ($< 1\%$ of the total film area). For the data shown in Fig. 3.1, the range included in the fit corresponds to times $t < 35000$ s $\sim 4\tau$. The quality of the fit to the initial stages of the data is very good, as can be seen from the inset to Fig. 3.1, giving the following best fit parameter values: $\tau = 8560 \pm 10$ s, $A_1 = 0.102 \times 10^6$ μm, $A_2 = 12.3$ Pa and $C_o = 0.0736$ μm/s.

It is important to note that the statistical noise in the data varies inversely as ΔP. An increase in the signal-to-noise ratio, and therefore a more sensitive measure of the onset of hole formation, could be obtained by increasing ΔP, but this would increase the

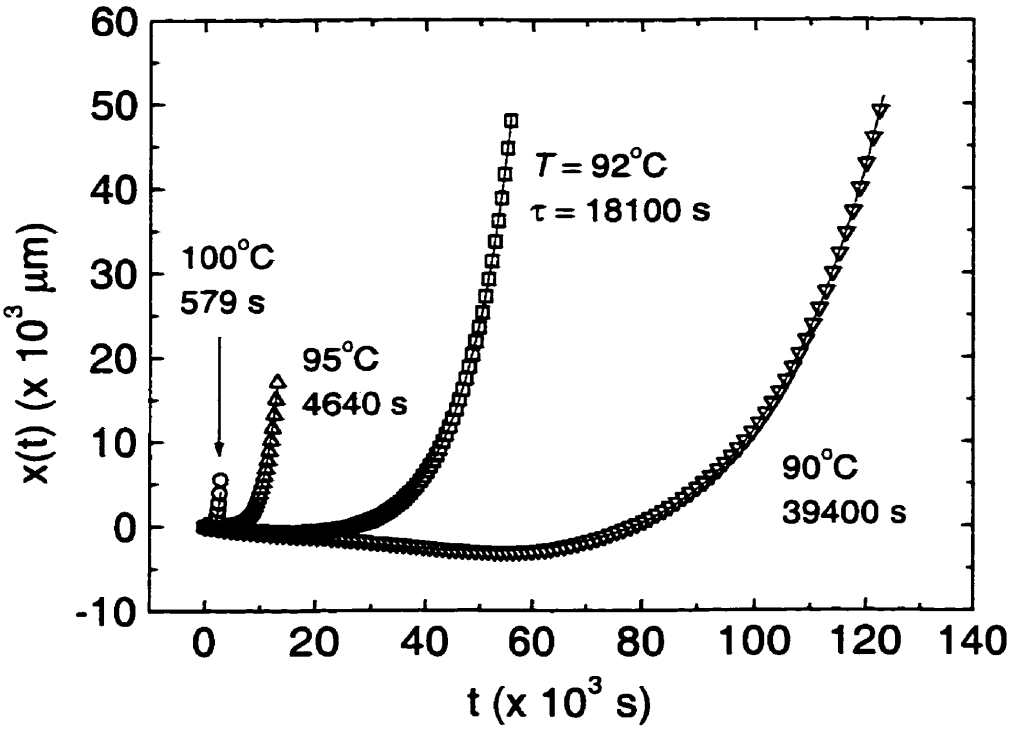

Figure 3.2: Time dependence of the piston position $x(t)$ for four different PS films held at the temperatures indicated. The τ values are given on the graph, while the other parameter values of the best fit to eqn. (2.32) are listed in Table 3.1.1.

in-plane stress in the film which could possibly affect the dynamics of hole formation. For the present measurements, we chose ΔP to be as small as possible so as to gently bow the film.

We have measured the characteristic growth time τ of the holes in 18 different PS films at different temperatures. Figure 3.2 shows the time dependence of the piston position $x(t)$ for four representative films, each measured at a different temperature: 90°C, 92°C, 95°C and 100°C. The temperature and τ values for each data set are indicated in the figure. Table 3.1.1 gives the parameter values for the four fits in Figure 3.2. Note the large spread in τ values.

We obtain a plot of the characteristic growth time τ as a function of temperature

Table 3.1: Parameter values of the best fit curves to eqn. (2.32) in Figure 3.2.

T (°C)	h (nm)	τ (s)	C_o (μm/s)	A_1 (μm)	A_2 (Pa)
90	65	39400 ± 100	0.0865	8.49×10^7	15.4
92	67	18100 ± 14	0.0767	1.16×10^8	9.97
95	66	4640 ± 20	0.119	9.44×10^6	80.5
100	63	579 ± 25	0.0076	5.49×10^5	13.9

T, shown in Figure 3.3. There are two sets of data shown in this graph. The first (solid circles) was obtained for a very small pressure difference of $\Delta P = 0.05$ torr. The pressure difference was then doubled (open triangles) to show that there is no change in the measured τ values. This demonstrates that the stress in the sample created by the small pressure difference does not affect the formation and growth of the holes in the films. The solid curve is a best fit to the empirical Vogel-Fulcher function using a value of the Vogel temperature which is reduced from the bulk value for PS (see section 3.2 for details). The errors in the τ values, as determined by the best fit to eqn. (2.32), are smaller than the size of the symbols, while the scatter in the data gives the reader a feel for the sample-to-sample variation in the measurement.

3.1.2 Microscopy Results

The presence of holes was verified at the conclusion of a run of the DPE by quenching the sample to room temperature and measuring it using an Olympus BX-60 reflected light microscope. Figure 3.4 shows an optical micrograph of a 64 nm thick freely-standing polystyrene film that was held at $T = 90$°C for 12 hours. After 12 hours, there are many holes ($\sim$ 13000 holes/mm^2) ranging in size from 0.5 μm to 2 μm in diameter. The gas flow through the film will be dominated by the large holes whose size is an order of

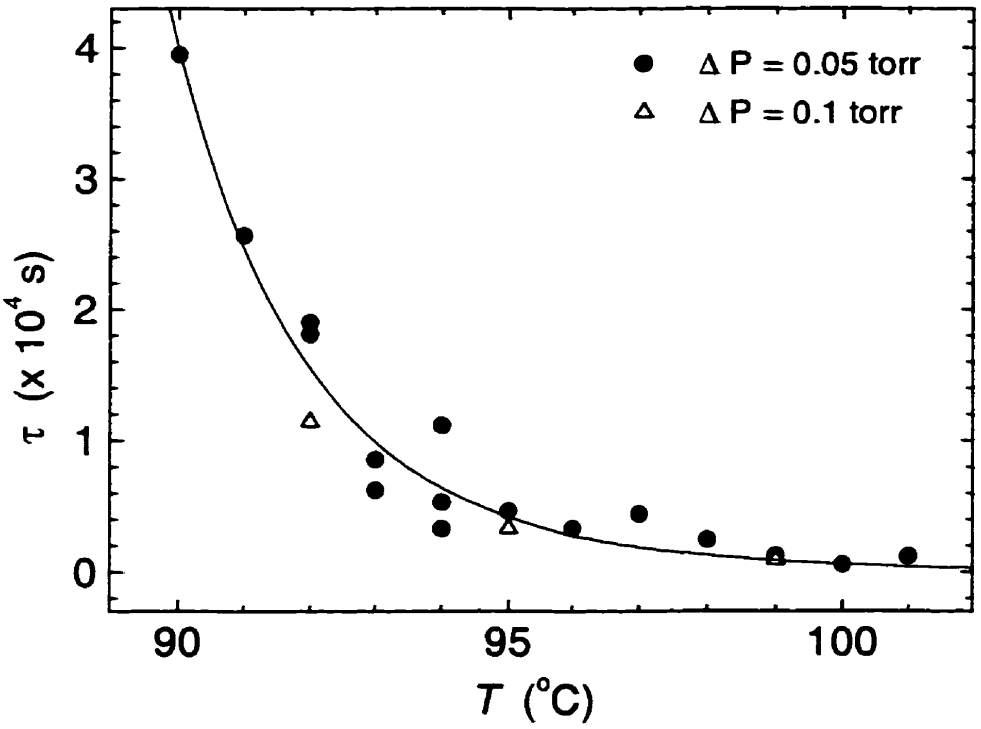

Figure 3.3: Plot of the characteristic growth time τ as a function of temperature T for freely-standing PS films. The solid curve is a best fit to the Vogel-Fulcher function allowing for a reduction of the Vogel temperature from the bulk value (see text for details).

magnitude larger than the mean free path ℓ of the gas molecules such that the effusion approximation is not valid. This provides justification for limiting the range of the data used in the fitting procedure to the initial stages, as described in section 3.1.1.

After each run, the freely-standing film was transferred onto a silicon wafer and its thickness was measured using ellipsometry. Additional features can been seen for the supported film compared to those visible for the freely-standing film because of the improved optical contrast in the presence of the silicon substrate. In particular, many closely-spaced dark spots, ~ 1 μm in size, are visible over the entire surface of the film. Figure 3.5 shows an optical micrograph of a PS film transferred onto a silicon substrate.

To characterize the dark spots, we measured one of the samples using a Nanoscope III

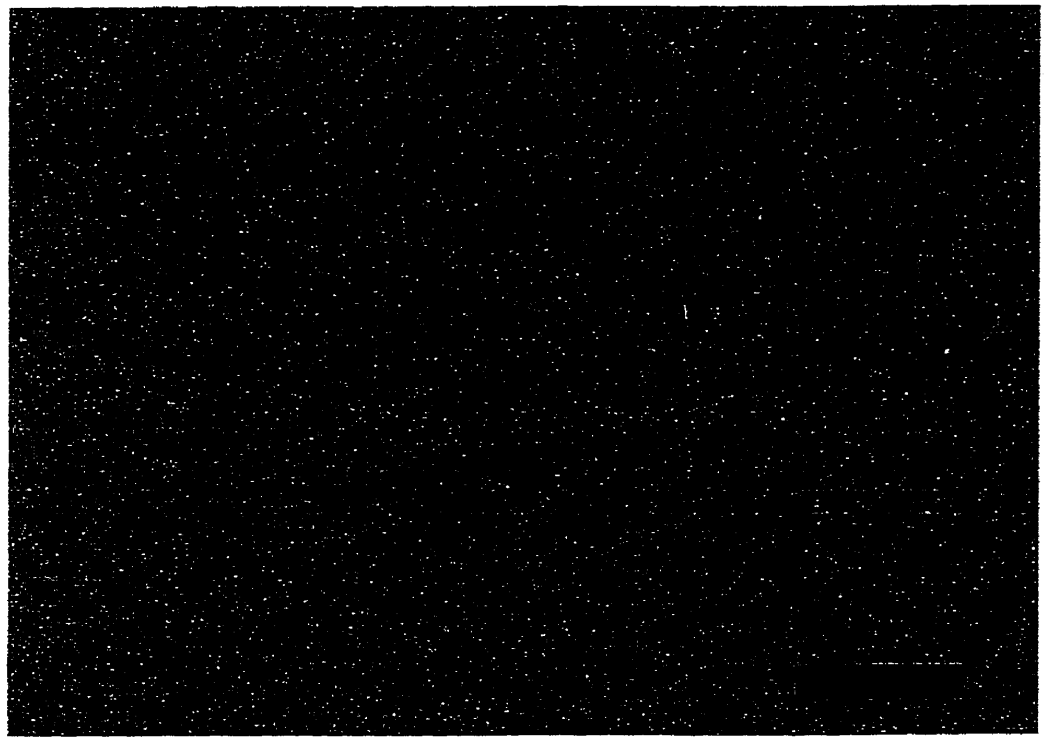

Figure 3.4: Optical micrograph of a polystyrene freely-standing film 64 nm thick after being held at $T = 90°C$ for 12 hours. The holes are approximately 0.5 μm to 2 μm in diameter ($\sim$ 13000 holes/mm^2). The entire image corresponds to a sample area of 127.5 μm $\times$95.6 μm and the bar indicates a length of 20 μm.

Atomic Force Microscope (AFM). Figure 3.6 shows an AFM image of the same polystyrene film supported on silicon as in Figure 3.5 ($h = 67$ nm, held at 92°C for 21 hours). The dark spots are small bumps that are $\sim$ 15 nm in height, $\sim$ 1 μm in diameter, and roughly equally spaced by $\sim$ 1.5 μm.

We can calculate the spacing λ between holes for spontaneous hole formation using [1]

$$\lambda = 2\pi\sqrt{\frac{2\pi\epsilon h^4}{A}}, \tag{3.1}$$

where ϵ is the surface tension, h is the film thickness and A is the Hamaker constant. Taking reasonable values for the above parameters ($\epsilon = 36 \times 10^{-3}$ N/m, $h = 65 \times 10^{-9}$ m,

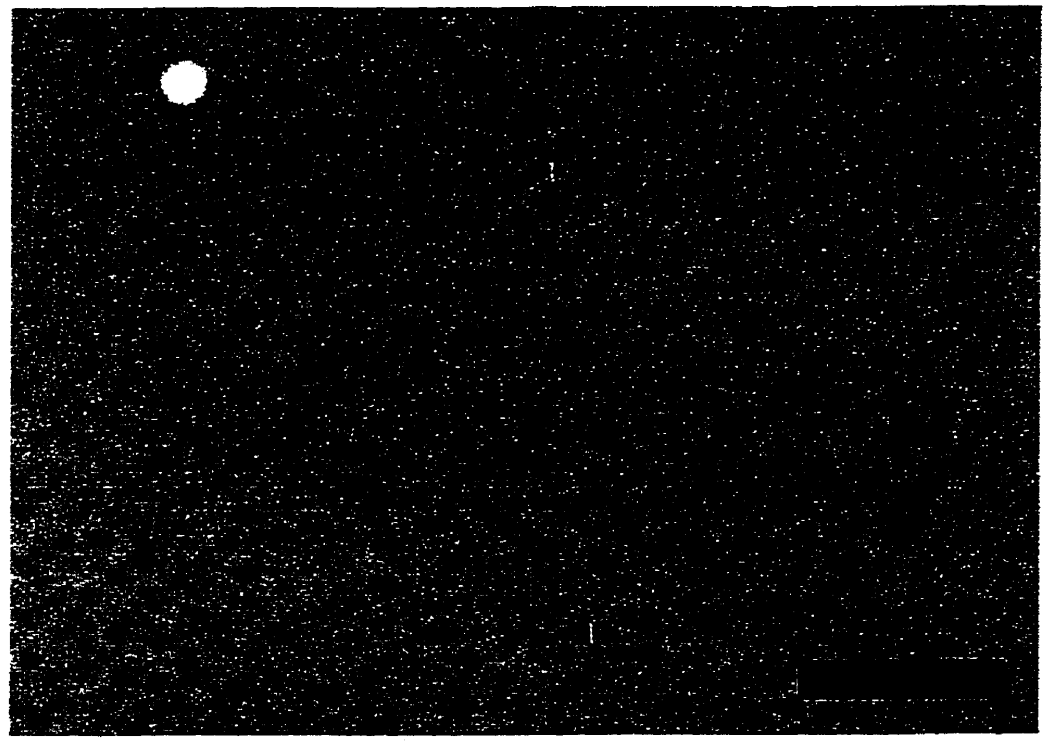

Figure 3.5: Optical micrograph of a polystyrene film 67 nm thick transferred onto silicon after being held at 92°C for 21 hours in the freely-standing state. There is a single hole in the top left corner (white circle), whereas the rest of the image is covered with dark spots of $\sim 1\mu$m in size. The bar indicates a length of 10 μm.

$A = 6.6 \times 10^{-20}$ J [13]), we calculate a wavelength of $\lambda = 1.5$ μm, which is comparable to the spacing between the small bumps.

3.2 Discussion

From our measurements of the characteristic growth time, we are able to determine the viscosity at the edge of the holes in the freely-standing film (see section 1.2.2). Equation (1.11) gives the viscosity in terms of the characteristic growth time τ, the surface tension ϵ, and the film thickness h. We measure the film thickness before the DPE using ellipsometry. We take the film thickness to be constant during hole growth despite the fact that the instantaneous elastic response of the viscoelastic film leads to uniform thickening. This is

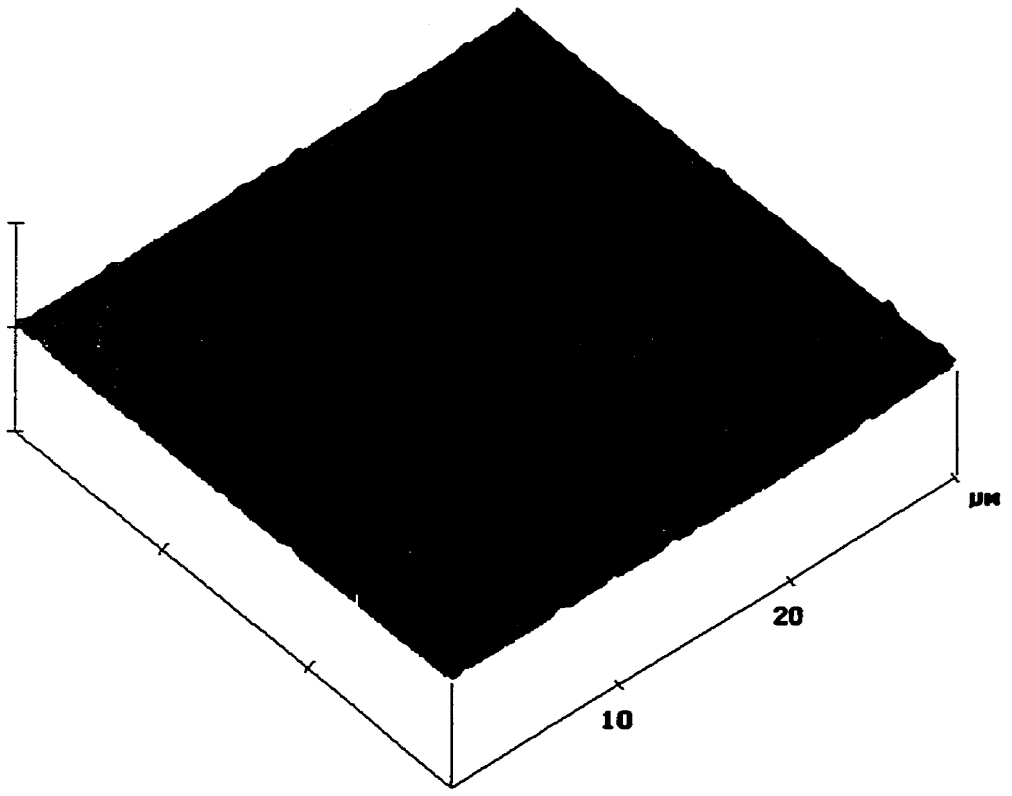

Figure 3.6: Atomic force micrograph of the same polystyrene film supported on silicon as in Figure 3.5 ($h = 67$ nm, held at 92°C for 21 hours). The bumps are ~ 15 nm in height, ~ 1 μm in diameter, and roughly equally spaced by ~ 1.5 μm. The entire image is 30 μm $\times$ 30 μm.

a reasonable approximation for the initial stages of hole growth, since the total hole area is less than 1% of the total film area (~ 12 mm^2). Also, we take the surface tension ϵ to be that of bulk polystyrene [14][1]: we assume that the surface tension is the same for all films and is not affected by confinement of the polymer molecules. This is a reasonable approximation because the length scale associated with surface tension (~ 1 nm) is much smaller than the thickness of the film ($h \sim 65$ nm). Thus from our hole measurements, we are able to obtain accurate values of the film viscosity. A plot of viscosity η versus temperature T is shown in Figure 3.7 based on the data shown in Figure 3.3. Again the

[1] $\epsilon = 40.7$ mN/m at 20°C with a change of -0.072 mN/m per K.

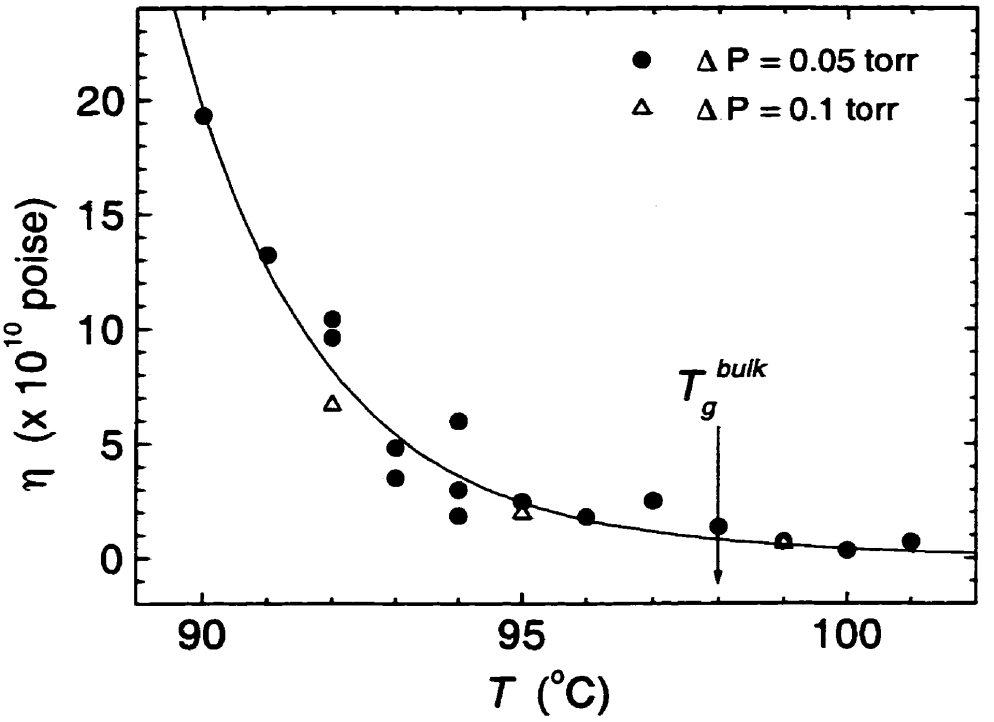

Figure 3.7: Plot of the viscosity η as a function of temperature T for freely-standing PS films. The solid curve is a best fit to the Vogel-Fulcher function allowing for a reduction of the Vogel temperature from the bulk value (see text for details).

same two sets of data, collected for $\Delta P = 0.05$ torr (solid circles) and 0.1 torr (open triangles), are shown in the graph.

As expected, the data shown in Figure 3.7 clearly shows the trend of increasing viscosity with decreasing temperature. However it is surprising that we are able to measure the viscosity for temperatures as low as 90°C, which is 8°C below the bulk value of the glass transition temperature T_g^{bulk}. This result demonstrates that the polymer chains in very thin freely-standing PS films have considerable mobility at temperatures well below T_g^{bulk}. However, it is important to note that the temperatures at which hole formation and growth is observed are much larger than the T_g value for the freely-standing PS films ($T_g \sim 55$°C).

To explain the viscosity data, we consider two different possibilities. First of all, we expect the temperature dependence of the viscosity of a polymer melt to follow a Vogel-Fulcher function (see section 1.1):

$$\eta = B\, e^{\frac{T_A}{T - T_V}} \tag{3.2}$$

in which T_A is the 'activation temperature' and T_V is the 'Vogel temperature' which is typically 50°C below the glass transition temperature [2]. This is an empirical relationship which is found to hold for bulk polymers. Since T_g for our films is reduced from the bulk value, it is reasonable to expect that the Vogel temperature is also reduced. In fact, we obtain a good fit to the viscosity data (shown as the curve in Figure 3.7) using a value of the Vogel temperature T_V that is reduced from the bulk value by an amount which is comparable to the reduction in T_g. The data has been fit to the Vogel-Fulcher function, fixing the activation temperature T_A at the bulk value for polystyrene ($T_A = 1800$ K) [15]. The best fit to the data was found using a Vogel temperature $T_V = 300 \pm 1$ K (27°C), which is lower than the bulk value by 22°C. Recall that these films have a glass transition temperature T_g that is 40°C less than bulk $T_g = 98$°C. The reduction of T_V by an amount comparable to the reduction in T_g is similar to that found for structural relaxation measurements of freely-standing PS films [16]. In these measurements, the average structural relaxation time, which is also described by a Vogel-Fulcher function [2], was well-described by bulk parameters except for a reduction in T_V equal to the reduction in T_g for the films.

The second possible explanation of the viscosity data is related to the fact that the magnitude of the measured viscosity ($\sim 10^{10} - 10^{11}$ poise) is several orders of magnitude

less than that typically associated with the glass transition temperature (10^{13} poise) [2]. This reduction in the viscosity is most likely due to nonlinear viscoelastic effects which are very important in the presence of high shear rates or highly entangled chains (see section 1.2.2). As discussed by Graessley [3], the importance of shear strain rate effects on the viscosity can be seen by calculating the dimensionless shear strain rate, equation (1.6),

$$\beta = \left(\frac{\eta_o M_w}{\rho R T}\right)\dot{\gamma} \ , \tag{3.3}$$

where R is the gas constant. The dimensionless shear rate β includes the effects of molecular weight M_w, density ρ, temperature T and the zero shear rate value of the viscosity η_o, enabling comparisons between different polymers. The shear strain rate $\dot{\gamma}$ is obtained from the characteristic growth time using $\dot{\gamma} = 2/\tau$ (see section 1.2.2). For bulk melts of PS with molecules of high molecular weight M_w and narrow M_w distribution, it has been found empirically that for small shear rates, $\beta < 10$, viscosity is constant and equal to the zero shear rate value η_o. However for $\beta > 10$, *nonlinear* effects become increasingly important causing large reductions in the viscosity, an effect commonly referred to as 'shear thinning' ([3], see section 1.1).

The previous study on hole formation and growth ([6], see section 1.2.2) measured freely-standing PS films ($M_w = 767 \times 10^3$) at 115°C. For film thicknesses $h > 96$ nm, τ values were observed in the range from 168 s to 6640 s which corresponds to β values in the range ~ 40 to ~ 1500, thus indicating that the study was probing the *nonlinear* viscoelastic regime. In the present study, hole formation and growth in freely-standing PS films with $M_w = 2240 \times 10^3$ and thickness $h \approx 65$ nm are measured at temperatures equal to and less than the bulk value of the glass transition temperature T_g^{bulk} where τ values

in the range from 756 s to 39400 s are observed. It is not possible to directly calculate a β value for the present study, since the zero shear rate viscosity η_o is unknown for these PS films that have a glass transition temperature which is reduced from the bulk value T_g^{bulk}. However, it is possible to compare our work to the previous study in order to get a feel for the importance of nonlinear viscoelastic effects. In equation (3.3), β is directly proportional to the product $\eta_o M_w$, and given that η_o scales like $M_w^{3.4}$ (see section 1.1), we expect $\beta \sim M_w^{4.4}$. For this study we have increased the molecular weight M_w by a factor of 2.9, thus β should be larger by a factor of 100. The film thickness h has been reduced increasing the shear stress $\sigma = 2\epsilon/h$ at the edge of the hole. In addition, the lower measurement temperature results in larger viscosities. All of these factors act to increase β. Thus despite the fact that in the present measurements we are measuring τ values that are larger than those measured in the study of ref. [6], which corresponds to shear rates that are smaller by an order of magnitude, we expect nonlinear viscoelastic effects to be even more important in the present study.

Overall, the viscosity data shown in Figure 3.7 are likely due in part to both of these effects: a reduced value of the Vogel temperature caused by the reduction in the glass transition temperature, and the effects of nonlinear viscoelasticity. However, it is unknown whether or not the empirical Vogel-Fulcher function is valid in the nonlinear viscoelastic regime. Future work will attempt to decouple these two effects to achieve a deeper understanding of the viscosity behavior of freely-standing PS films.

It should be noted that the present use of the DPE appears to be similar to a physical aging experiment [17] in that the film is being held at a temperature less than T_g^{bulk}. In physical aging experiments, one expects to measure a decrease in the free volume, and

therefore an increase in density, with time. This produces an increase in viscosity with time as the system relaxes to its equilibrium structure. In the DPE, an increase in viscosity over time would result in an increase in the measured τ value with time. However, we obtain an excellent fit using a single τ value to the $x(t)$ data (see Fig. 3.1) for which the effusion approximation is known to be valid. In the present DPE measurements of very thin, freely-standing PS films, the film is held at temperatures that are well above the T_g value of the film, such that physical aging effects are not expected to occur.

There is one last puzzling point that is worth mentioning. When comparing this hole formation study on PS films with a reduced value of $T_g \approx 55°C$ to the previous study on PS films with the bulk value of T_g, one would have expected holes to form at temperatures even less than 90°C. The previous study measured hole formation at 17°C above the glass transition temperature of the film $T_g^{bulk} = 98°C$. Yet this study measures hole formation occuring only at temperatures $> 35°C$ above the glass transition of the film $T_g \approx 55°C$. In addition, the best fit to the viscosity data is obtained for a Vogel temperature that is reduced by only 22°C for films that have a glass transition temperature that is reduced by 40°C. This discrepancy between the temperature at which hole formation occurs and the T_g value of a freely-standing film suggests the following: the terminal flow region remains unchanged while the glass-rubber transition is shifted to shorter times leading to a longer plateau in the compliance curve (Figure 1.2). A longer plateau in PS films with reduced values of the glass transition temperature would imply a greater time (or, equivalently, temperature) difference between the onsets of segmental and chain mobilities.

4

Summary and Conclusions

We have designed and constructed a sensitive Differential Pressure Experiment (DPE) which allows us to observe the onset of hole formation in thin freely-standing polystyrene (PS) films. The presence of holes is observed as a flow of air across the PS film which is held at a fixed elevated temperature. The DPE is sensitive to total hole areas of $\sim 30\ \mu\text{m}^2$ over the entire surface of the film (4 mm in diameter).

Using the DPE, we have measured hole formation in freely-standing PS films that have a reduced value of the glass transition temperature of $T_g \sim 55°\text{C}$ which is $40°\text{C}$ less than the bulk value of the glass transition temperature $T_g^{bulk} = 98°\text{C}$. By measuring the characteristic growth time τ at different temperatures in 18 different PS films, with thicknesses h between 61 nm and 69 nm, we have obtained a plot of viscosity as a function of temperature. These measurements have been performed at temperatures equal to and less than the bulk value of the glass transition temperature.

The viscosity data we have collected can be explained by two possible effects. The first interpretation fits the data to the empirical Vogel-Fulcher function using a value of the Vogel temperature which is reduced by $22°\text{C}$ from the bulk value of $49°\text{C}$. The second explanation is related to the effects of nonlinear viscoelasticity which have been seen, in previous hole formation studies on PS films [6], to be quite important. It is likely that

both these effects are responsible for the observed results such that more work is required in order to decouple them.

This hole formation study on PS films, with a reduced value of the glass transition temperature, suggests a larger discrepancy between segmental and chain mobility compared to the previous study on PS films with bulk values of T_g [6].

4.1 Future Work

Future work will start by expanding the current viscosity results to different film thicknesses, including thicker films that have the bulk value of T_g, in hopes of separating the effect of reduced Vogel temperature from nonlinear viscoelasticity. This work can be broadened to include different molecular weights, as well as other polymers.

The DPE also provides a good base for future experiments. By reflecting a laser beam from the surface of the film, the radius of curvature can be measured as a function of pressure and temperature enabling determination of the glass transition temperature and thermal expansion properties within the plane of the film. By combining the DPE with ellipsometry, for instance, which is sensitive to changes perpendicular to the plane of the film, questions about possible anisotropy in the film can be investigated. In addition, a small speaker could be implemented in the DPE, to excite different resonant modes of vibration in the freely-standing films to probe the mechanical properties of the films.

References

[1] A. Vrij, F. Hesselink and H. Van Der Tempel, Koninkl. Nederl. Academie van Wetenschappen Amsterdam. B, **73**, 124 (1970).

[2] G. Strobl *The Physics of Polymers: Concepts for Understanding Their Structures and Behaviour*, Second Edition (Springer-Verlag, Berlin, 1997).

[3] W.W. Graessley, Adv. Polym. Sci. **16**, 1 (1974).

[4] J.A. Forrest, K. Dalnoki-Veress, J.R. Stevens and J.R. Dutcher, Phys. Rev. Lett. **77**, 2002 (1996).

[5] J.A. Forrest, K. Dalnoki-Veress and J.R. Dutcher, Phys. Rev. E **56**, 5705 (1997).

[6] K. Dalnoki-Veress, B.G. Nickel, C. Roth and J.R. Dutcher, Phys. Rev. E **59**, 2153 (1999).

[7] G. Debrégeas, P. Martin, and F. Brochard-Wyart, Phys. Rev. Lett. **75**, 3886 (1995).

[8] G. Debrégeas, P.-G. de Gennes, and F. Brochard-Wyart, Science **279**, 1704 (1998).

[9] C.V. Boys, *Soap Bubbles* (Dover, New York, 1959).

[10] E.I. Bromley, J.N. Randall, D.C. Flanders and R.W. Mountain, J. Vac. Sci. Technol. B **1**, 1364 (1983).

[11] M.G. Allen, M. Mehregany, R.T. Howe and S.D. Senturia, Appl. Phys. Lett. **51**, 241 (1987).

[12] K. Huang, *Statistical Mechanics* 2nd ed. (John Wiley & Sons, New York, New York, 1987).

[13] J.N. Israelachvili, *Intermolecular & Surface Forces* , Second Edition (Academic Press, San Diego, 1991).

[14] *Polymer Handbook*, Third Edition, eds. J. Brandrup and E.H. Immergut (Wiley, New York, 1989).

[15] A. Sahnoune, F. Massines, and L. Piché, J. Polym. Sci. B: Polym. Phys. **34**, 341 (1996).

[16] J.A. Forrest, C. Svanberg, K. Révész, M. Rodahl, L.M. Torell and B. Kasemo, Phys. Rev. E 58, R1226 (1998).

[17] L.C.E. Struik, *Physical Aging in Amorphous Polymers and Other Materials* (Elsevier, Amsterdam, 1978.)

A

Components of the Differential Pressure Experiment

A.1 Computer Code

The computer code was written using Borland Turbo C++ (version 3.0). A 16-bit executable file called **membrane.exe** is generated from **membrane.prj** with **membrane.cpp**. Figure A.1 shows the start-up menu of the program.

```
                MEMBRANE DEFLECTION EXPERIMENT
               --------------------------------
                        Guelph BLS Polymer Group, 1998.

      1.  Set gain of pressure sensor.       (HIGH)
      2.  Set target pressure.               (0.00000 torr)
      3.  Set microstepping.                 (32 microsteps)
      4.  Maintain pressure...
Record data to a file:
      5.  Set time interval between writes.  (60 sec)
      6.  Set file name for output.          (output.dat)
      7.  Maintain pressure with file output...
      0.  Exit.
Enter choice (1-7 or 0):
```

Figure A.1: Main menu of program **membrane.exe** that runs the Differential Pressure Experiment.

Option 1 changes the gain setting from HIGH (-1.25 to $+1.25$ V) to LOW (-10 to $+10$ V). The high gain setting allows for higher pressure resolution without being limited by the digital levels of the analog to digital converter of the Keithley data acquisition card (0.006 torr LOW gain resolution vs 0.0006 torr HIGH gain resolution). The pressure sensor has a resolution of 0.001 torr.

Option 2 sets the target differential pressure to be maintained by the system.

Option 3 selects the desired degree of microstepping of the stepper motor. This allows for variation of the pressure change caused by each step of the piston. It has been found that settings coarser than 32 microsteps cause vibration in the polymer film as the piston moves.

Option 4 runs the program with the above parameters maintaining the desired target pressure by adjusting the position of the piston back and forth. There is a continuous display showing the target pressure, the measured pressure, and a counter in microsteps which is set to zero when this option is selected.

Option 5 sets how often output is written to a file.

Option 6 sets the output file name (only 8 characters plus the extension).

Option 7 is identical to Option 4, but includes data output to a file. The continuous display also includes the time in seconds and a count rate in microsteps per second updated every 10 s.

The main loop of the program, which is executed continuously during operation of Options 4 and 7, starts by reading a value from the pressure sensor. This reading, an

integer value from 0 to 4096, is converted to a voltage using the following equation:

$$\text{Voltage} = \frac{(\text{count} - 2048) \times \text{span}}{4096},$$

where span = 20.0 V for a gain of 1 (LOW) and 2.5 V for a gain of 8 (HIGH). This produces a bipolar voltage from -1.25 to $+1.25$ V for HIGH gain or -10 to $+10$ V for LOW gain, which is then converted to a pressure value. The measured pressure reading is then compared to the target pressure value and a decision is made whether the piston should move forward, backward, or not at all. Based on this decision, a digital output is sent to the stepper motor which acts accordingly. Finally the screen display and data file (for Option 7) are updated and the loop is started again.

The program loop is executed nearly 150 times a second which sets the response time of the system. Each FULL step of the stepper motor corresponds to 3.175 microns which produces a corresponding change in pressure of $\Delta P = 0.016$ torr (see Table A.1)[1].

Table A.1: Change in pressure ΔP for different stepping options of stepper motor.

MICRO STEP	ΔP (torr)
Full	0.016
Half	0.008
4	0.004
8	0.002
16	0.001
32	0.0005
64	0.0002
128	0.0001

A.2 Data Acquisition Card

A **Keithley DAS-1602 data acquisition board** is used to read and control the differential pressure in the Differential Pressure Experiment. Despite the many abilities of the

[1] Note the pressure sensor has a resolution of 0.001 torr.

DAS-1602 board we are only using it to read in analog values and output digital pulses.

The DAS-1602 board can be easily controlled through the program code by calling various preset Keithley card functions. For our purposes only four of these are required.

- **K_OpenDriver("DAS1600", "DAS1600.cfg", &Driver)** and **K_GetDevHandle(Driver, 0, &Device)** are used to initialize the DAS-1602 Keithley card according to the configuration file **DAS1600.cfg**. The configuration file is created using the utility **CFG1600.exe**.

- **K_ADRead(Device, channel, gain, value)** is used to read in an analog value from the pressure sensor and **K_DOWrite(Device,channel,value)** is used to output the required digital pulses to the stepper motor.

There are a number of external files required for the operation of the DAS-1602 board:

- Three *.dll files are to be put in the windows directory. **c:/windows/... das1600.dll, dasshell.dll, dassuprt.dll**

- Reference to the file **dasdecl.h** needs to be included at the beginning of the program code as **#include "dasdecl.h"**.

- Links to the two library files **Dasimp.lib** and **D1600imp.lib** need to be made in the program. D1600imp.lib is actually redundant as it is only needed for DAS1600_...() commands. For each DAS1600_...() command, there exists an equivalent command that can be used in its place, i.e. K_OpenDriver() is equivalent to DAS1600_DevOpen().

- **DAS1600.cfg**, which has already been mentioned, contains the configuration information for the board and is read on initialization of the program.

Table A.2: Contents of file **DAS1600.cfg**.

```
Board          0
Name           DAS1602
Address        &H200
ClockSel       10MHz
WaitState      NO
ADChanMode     Bipolar
ADChanConfig   Differential
DAC0Mode       Bipolar
DAC1Mode       Bipolar
DAC0Ref        -5.0 (C0A00000)
DAC1Ref        -5.0 (C0A00000)
DMAChannel     3
IntLevel       7
PortA          Output
PortB          Input
PortCL         Input
PortCH         Input
NumOfEXP16     0
NumOfEXPGP     0
NumOfEXP1600   0
NumOfSSH       0
ADChannels     8
```

The configuration utility **CFG1600.exe** indicates the required dip switch settings on the DAS-1602 board based on the information in the configuration file. These settings are shown in Figure A.2.

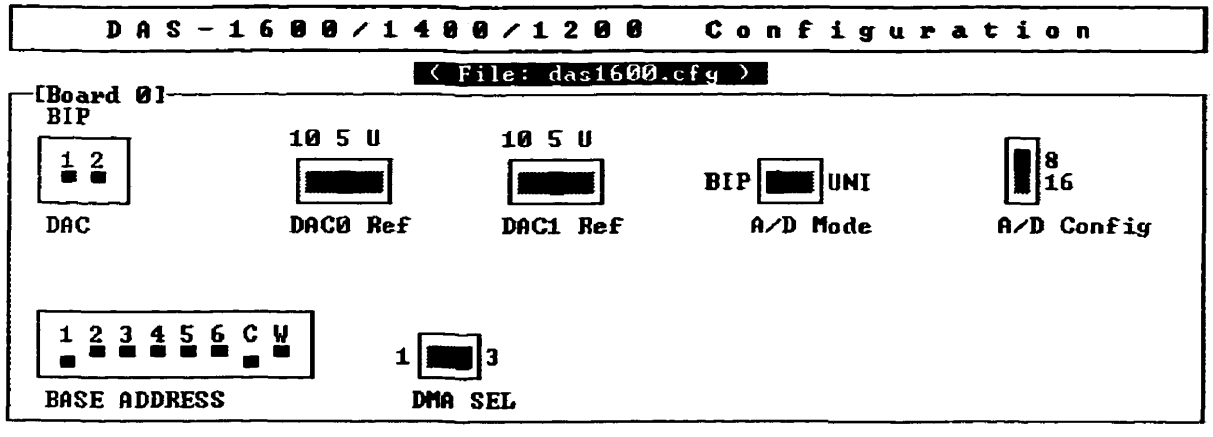

Figure A.2: Dip switch configuration for the Keithley DAS-1602 data acquisition board.

In the configuration file, Port A, located on the programmable input/output (PIO) Cable Connector, has been configured as output for use with the stepper motor. A digital output is always sent to channel 0 where each bit of the digital output represents a different pin number on the connector. When Port A is designated as output, the first 8 bits (or right most bits) are sent to PA 0 through PA 7 respectively. To control the stepper motor we only need 6 outputs which are listed here and will be described in the next section on the stepper motor (section A.3).

Table A.3: Outputs of Port A which used to control the stepper motor.

PA 0	PIN 37	clock
PA 1	PIN 36	direction
PA 2	PIN 35	enable
PA 3	PIN 34	microstepping
PA 4	PIN 33	microstepping
PA 6	PIN 31	microstepping

PA 5 PIN 32 is not functioning properly: it always reads low regardless of the input from the computer. Thus PA 6 PIN 31 was used in place of it. DIG COM PIN 19 is used as the ground for the stepper motor controls PA 0 to PA 2 and DIG COM PIN 17 is used as ground for the microstepping (PA 3, PA 4 and PA 6).

Input from the pressure sensor is read through the Main I/O Connector on Ch 0 HI IN PIN 37, the first analog channel. Because ADChanConfig is set to differential in the configuration file the input signal is measured as the difference between Ch 0 HI IN PIN 37 and Ch 0 LO IN PIN 18. This setup allows for the minimization of noise when Ch 0 LO IN PIN 18 is connected to ground (LL GND PIN 19).

It is convenient to have the inputs and outputs separated between the Main I/O Connector and PIO Cable Connector. Because of this, the Main I/O Connector is connected only to the pressure sensor and the PIO Cable Connector is connected to the electronics

box which drives the stepper motor.

A.3 Stepper Motor

A **model 801AM linear actuator** (stepper motor) with anti-backlash, from American Scientific Instruments (AMSI) Corporation, moves the piston in and out. This motor is controlled by a **7200-DB driver board** that requires six digital inputs.

clock The stepper motor takes one step every clock pulse. It steps on the negative edge. Typically, the pin is kept high until a step is issued by dropping the pin low for at least 0.5 microseconds.

direction High moves the motor clockwise and low moves counter-clockwise.

enable High means the motor is on, while low disables it. This allows for the motor to be turned off via the program code. Currently the computer code does not make use of this feature, so the pin is always kept high.

microstepping Three pins mimic the dip switch setting to control the level of microstepping. For computer control, the dip switches must be set to "OFF" (i.e. FULL STEPPING); otherwise, they override the output.

The stepper motor, which draws a phase current of 1.54 A, is powered directly from the 7200-DB driver board using a bipolar chopper drive (half-chopper) with the following wiring:

```
Q1    Red
Q2    Black
Q3    Green
Q4    White
```

Table A.4: 7200-DB digital input pin settings which control the step size of the stepper motor.

PIN INPUT	MICRO STEP
000	FULL
001	HALF
010	4
011	8
100	16
101	32
110	64
111	128

To be able to run the experiment overnight, we required an automatic turn-off feature to stop the program when the piston reaches the end of its travel, e.g. when the holes in the film get too big, such that the pressure difference across the film can no longer be maintained. We found that the stepper motor does not overheat when it is prevented from moving for 30 minutes. The program is set to stop if the pressure difference cannot be maintained for more than 60 seconds.

A.4 Electronics

A single box of electronics provides electrical connections to both the pressure sensor and stepper motor. The box contains two transformers, the 7200-DB driver board and a power supply circuit. The large transformer supplies 2 A of current at 20 V AC to the 7200-DB driver board to run the stepper motor. The smaller transformer supplies 0.15 A of current at 25 V AC which is rectified to ± 12 volts DC to power the pressure sensor and low pass filter (see section A.5). Figure A.3 shows the circuit diagram of the power supply which rectifies the transformer's 25 V AC and outputs ± 12 volts DC.

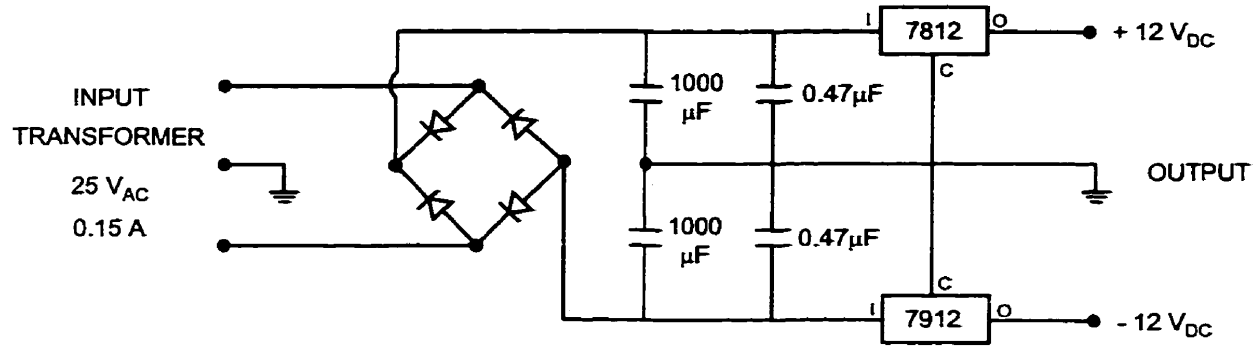

Figure A.3: Circuit diagram of power supply for pressure sensor.

A.5 Pressure Sensor

The **MKS Baraton Type 223B Pressure Transducer** measures differential pressure with a resolution of 0.001 torr over a full scale range of 10 torr and outputs a 0 to ± 1 volt signal which is linear with pressure. The sensor requires less than 25 mA of current at ± 12 volts DC which is supplied by the power supply circuit mentioned above (see section A.4).

The pressure sensor achieves 0.5% of full scale within 15 minutes of turning on the sensor. However, I have found that the pressure sensor requires approximately 2 hours after being turned on for its 'zero' reading to stabilize to a constant value. The electronics box (see section A.4) was wired with two switches so that the pressure sensor could be left on all the time, hence eliminating the need for warmup time. Zeroing of the pressure sensor can then be done by trimming its zeroing potentiometer, which should only be done when zero differential pressure across the sensor is assured, e.g. by opening the cross port value between both sides of the transducer. The pressure sensor's temperature stability is rated at 0.1% of full scale per degree Celsius. The sensor has a maximum overpressure of 20 psi (140 kPa). The volume on the P_x side (top half) is 1.3 cm^3, while on the P_R side (bottom half) the volume is 9.8 cm^3.

There is a high frequency oscillation superimposed on the pressure sensor output. The 50 mV oscillation at 12.5 kHz is clearly seen with an oscilloscope. The pressure sensor was designed to be read using a DC voltmeter which averages the input signal, however because the Keithley data acquisition card samples at such a fast rate, this high frequency oscillation is unacceptable.

We have built an external low pass filter which removes the high frequency oscillation on the pressure sensor output before it is read by the Keithley data acquisition card. Figure A.4 shows the circuit diagram of the first-order low-pass inverting active filter which is used.

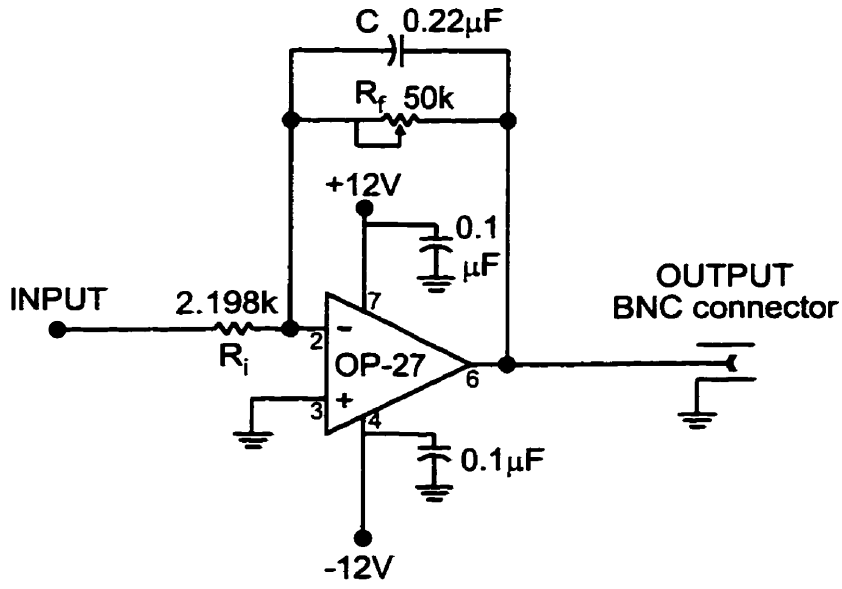

Figure A.4: First-order low-pass inverting active filter on the output of the pressure sensor.

The circuit contains 0.1μF decoupling capacitors to isolate the OP-27 amplifier from ground noise. All grounds are connected *separately* to the common, power supply ground, including the metal box grounding and sensor ground. The capacitor labeled C is a metallized film (orange) capacitor of about 0.2μF for a cutoff frequency of 40 Hz. It

is mounted on a socket for easy replacement. The 50 kΩ potentiometer R_f allows fine tuning of the gain. The gain of the amplifier is given by

$$\text{Gain} = -\frac{R_f}{R_i}.$$

Setting the 50 kΩ potentiometer at $\sim$ 20 kΩ gives a gain of 10^2. The voltage read by the Keithley data acquisition card is then 0 to ± 10 V, and linear with pressure. This setup allows for easy gain adjustment using the Keithley card from a LOW gain of 1 (-10 to $+10$ V) to a HIGH gain of 8 (-1.25 to $+1.25$ V). Typically experiments are done in the HIGH gain setting to get better pressure resolution, since this is limited by the digital levels of the analog to digital converter in the Keithley card.

To calibrate the gain of the low pass filter circuit, a DC voltmeter was connected to the pressure sensor output and the R_f potentiometer (see Figure A.4) was adjusted until the measured pressure output displayed on the computer screen matches the reading on the voltmeter.

A.6 Pressure Cell

Figure A.5 shows a technical drawing of the cylindrical pressure cell which was machined out of a single piece of aluminum. The figure is drawn to scale and indicates the inlet ports for the pressure sensor and thermocouple. A $1'' \times 3''$ kapton heater pad from Omega Instruments is wrapped around the central portion of the outside of the cell. The heater pad is held in place by two halves of an aluminum cylinder clamped together using Viton o-rings. The input voltage for the heater pad is 110 V AC and it has a maximum temperature of 200°C. The pressure cell was built with thin (thickness of $0.100''$) walls to

[2] Note capacitor C would have to be changed if R_f is changed considerably from $\sim$ 20 kΩ.

allow good heat transfer from the heater pad to the inside and to reduce the mass of the cell which increases the thermal response time. To get an air-tight seal of the top and base plates of the cell, o-ring seals were used. Access to the pressure sensor is obtained by attaching two 1/4″ OD stainless steel tubes using Torr-Seal adhesive. Despite the fact that Torr-Seal is not very durable, there exist few ways to attach stainless steel to aluminum.

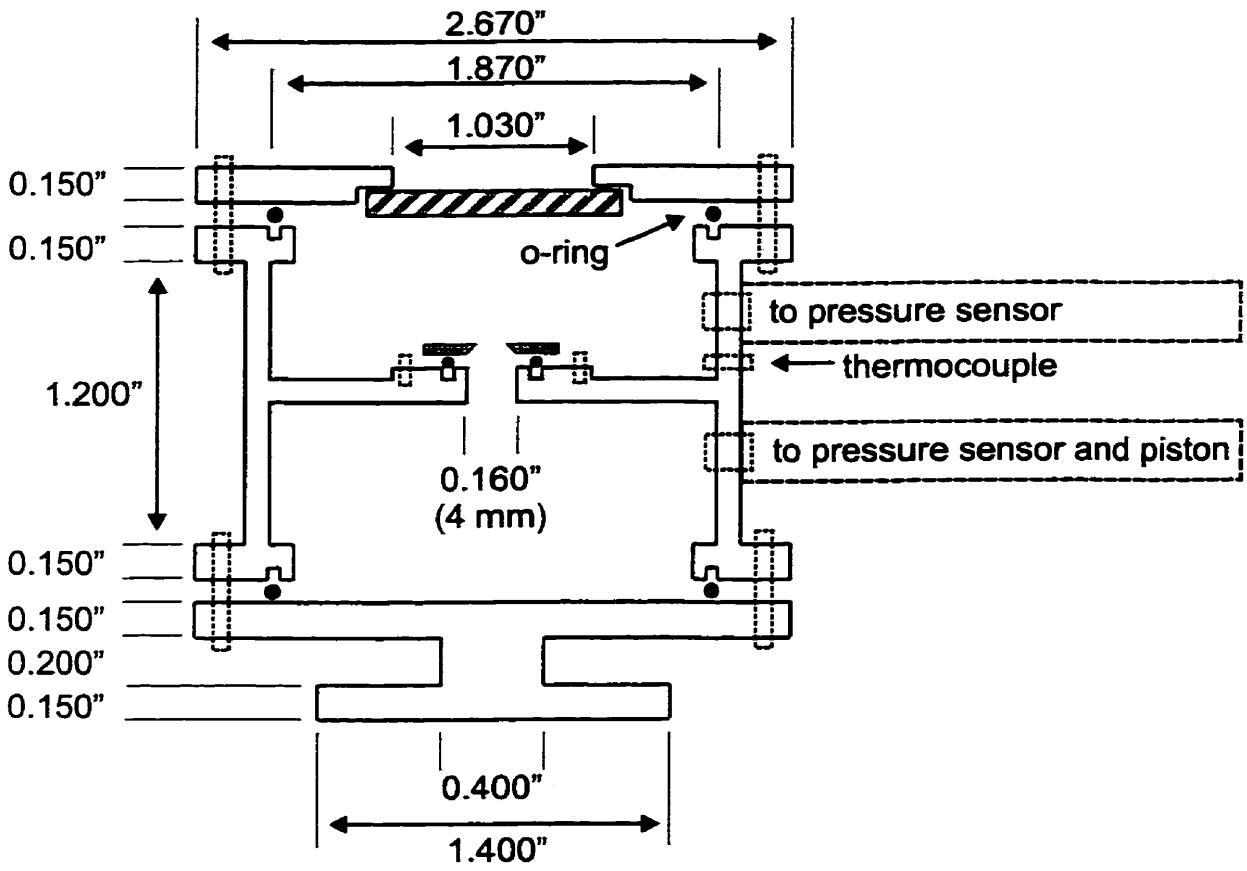

Figure A.5: Technical drawing of pressure cell with dimensions indicated.

A.7 Piston

A large 30 cm^3 syringe from Fisher with a Luer-Lok tip is used as the piston. To ensure that air does not leak out along the barrel, a thin oil is used to coat the barrel. At the end

of the syringe, the Luer-Lok connection is made using a bit of vacuum grease. Tubing is then attached directly to the Luer-Lok piece.

Originally tygon tubing was squeezed over the $1/4''$ OD of the Luer-Lok piece. However, this has been made more permanent by silver soldering a $1/4''$ OD piece of copper tubing several inches long onto the Luer-Lok connector. The copper tubing has a 90° kink in it because of the restrictions of the box dimensions[3]. The $1/4''$ OD copper tubing is then connected directly to a Swagelok fitting (see section A.8).

A.8 Valves and Tubing

The current setup of the experiment uses Swagelok valves and connectors with polyethylene $1/4''$ OD tubing between the cell, syringe and pressure sensor. However, the experimental apparatus has only recently been updated to this more permanent setup. Most of the data presented in this thesis was collected using glass Tees and Tygon $1/4''$ ID tubing which makes press-fit connections between the components with clamps used as valves. The system was thoroughly leak tested prior to data collection as well as after each upgrade of the system.

A.9 Thermocouple

A single **type T (copper-constantan) thermocouple** wire runs from the connector outside the cell to the sample position. The wire is fixed in place using Torr-Seal where it enters the cell and a large amount of wire ($\sim$ 1 m) is placed inside the cell to ensure that

[3] For temperature isolation from the rest of the lab, the entire experiment, except for the pressure cell, has been placed inside a large insulated box. This makes the experiment less sensitive to changes in the room ventilation, which is especially critical for long runs at low temperatures.

the thermocouple tip is at the sample temperature. At the point where the thermocouple wire enters the cell, the insulation around the wire has been removed. The Torr-Seal connection has to be made directly on the bare wire to prevent any leaks in the system. In forming this seal, it is necessary to ensure that no electrical contact is made between the thermocouple wire and the aluminum cell.

The current arrangement of a single wire Torr-Sealed into place was necessary for good thermal stability of the heater. Originally two separate pieces of copper and constantan wire were Torr-Sealed to form feed-through connections. A thick thermocouple wire was then used from the connector to the outside of the cell, and a thinner one from the inside to the thermocouple tip. This arrangement led to poor temperature stability that would fluctuate by several °C when trying to maintain a constant temperature.

A **Eurotherm Digital Temperature Controller Model 808** is used to regulate the temperature. The temperature controller works well with the same parameters as those used in other temperature controllers in the lab: **Prop** $= 5$, **Int.t** $= 50$, **dErt** $= 20$ and **Hct** $= 1.0$. Here is a brief description of these parameters.

Prop stands for *proportionality*. It is the proportionality factor for the amount of heat output based on the difference between the measured temperature and the setpoint. If Prop is too high the temperature will oscillate about the setpoint.

Int.t is a kind of integration time. When ramping up to a setpoint, Int.t reduces the heat output to prevent overshoot of the setpoint.

dErt is a kind of derivative time. This value determines the amount of heat output based on the rate of change of the temperature (derivative) near the setpoint. This

parameter is important in maintaining the setpoint temperature after it has been reached.

Hct is the cycle time for measuring the temperature and outputting heat, related to the response time of the system. Typically one second is a good setting.